BIOMECHANICAL EFFECTS OF RADIAL OPTIC NEUROTOMY

by

Sarajane Anita Hill

BSE, Geneva College, 2001

Submitted to the Graduate Faculty of

School of Engineering in partial fulfillment

of the requirements for the degree of

Master of Science in Mechanical Engineering

University of Pittsburgh

2007

UNIVERSITY OF PITTSBURGH

SCHOOL OF ENGINEERING

This thesis was presented

by

Sarajane Anita Hill

It was defended on

March 1, 2007

and approved by

Dr. William Slaughter, Associate Professor, Mechanical Engineering and Material Science

Dr. Qing-Ming, Wang, Associate Professor, Mechanical Engineering and Material Science

Thesis Advisor: Dr. Patrick Smolinski, Associate Professor, Mechanical Engineering and Material Science

BIOMECHANICAL EFFECTS OF RADIAL OPTIC NEUROTOMY

Sarajane Anita Hill, M.S.

University of Pittsburgh, 2007

A computer model was constructed to simulate the effect that radial optic neurotomy (RON) may have on central retinal vein biomechanics. Finite element analysis was used to determine the effect of RON on the size of central lumen. A model was constructed of the optic nerve, lamina cribosa and sclera and the material properties of the optic nerve tissue, intraocular pressure, and arterial pressure where varied. Comparison of the change in the diameter of the central lumen with and without RON showed that RON procedure did not result in a significant increase in diameter.

TABLE OF CONTENTS

LIST OF TABLES

LIST OF FIGURES

1.0 INTRODUCTION

A retinal vein occlusion is a blockage of a vein in the eye leading to hemorrhaging, fluid leakage and loss of circulation. This is the second most common blinding disorder in the US[1, 2] and central retinal vein occlusion (CRVO) is the most visually devastating disorder in this group. The pathophysiology of this disease is poorly understood[1, 3].

Although clinical scientists persever in researching therapeutic options for this highly prevalent condition, success in terms of visual outcome has been limited[2-4]. While there will be a lumen thrombus formation at some stage in CRVO, whether it is a primary or secondary event is unclear[3]. The site of the thrombus location and its ocular effects have been studied at various levels.

Efforts have been made to manipulate or interrupt the various stages both pharmacologically and surgically [6-8] In the surgical context there is still fierce debate as to the optimal management of an essentially vascular condition[4, 11, 12]. Relatively recently some authors have described a scleral compartment analogy for CRVO in which tissue pressure results in reduces the flow in the vein. Surgical techniques have been developed that attempt to decompress the lamina cribrosa through a radial incision or radial optic neurotomy (RON)[12]. RON is a specific technique which involves the creation of a radial incision at the level of the scleral ring, cribiform plate, and adjacent sclera of the optic disk. The rational for RON being that decompression may decrease venular flow resistance in this 'compartment'[13], improving the hemodynamics in the affected vein [14, 15]. Given the difficulty in executing a study on a technique

such as RON, we have used computational simulations to study the basic physical principles proposed to describe the utility of RON.

Here we have developed a finite element model of the relevant structures of the eye to examine the effects of RON from a biomechanical perspective. Finite element analysis has been used on similar type pressure vessel problems such as evaluating stress in aneurysms[17, 18] and recently been applied to the study of biomechanical aspects of the eye [19]. In this study, the structures of interest are the sclera, lamina cribosa and the optic nerve. The physical properties of the tissues and pressure loads were varied in order to assess the affects of these parameters on RON. The change in diameter of the central lumen was used as a measure of the effectiveness of the RON procedure in the treatment of the compartment syndrome.

2.0 METHODS

For the model of the eye, the globe of the eye was assumed to be a sphere and the optic nerve a cylinder such that the combined structure is axisymmetric. A three-dimensional model was constructed that contained the optic nerve, sclera and lamina cribosa. A plane of symmetry was taken along the lateral plane (y-z plane) so that only one half of the structure was modeled as shown in Figure 1.

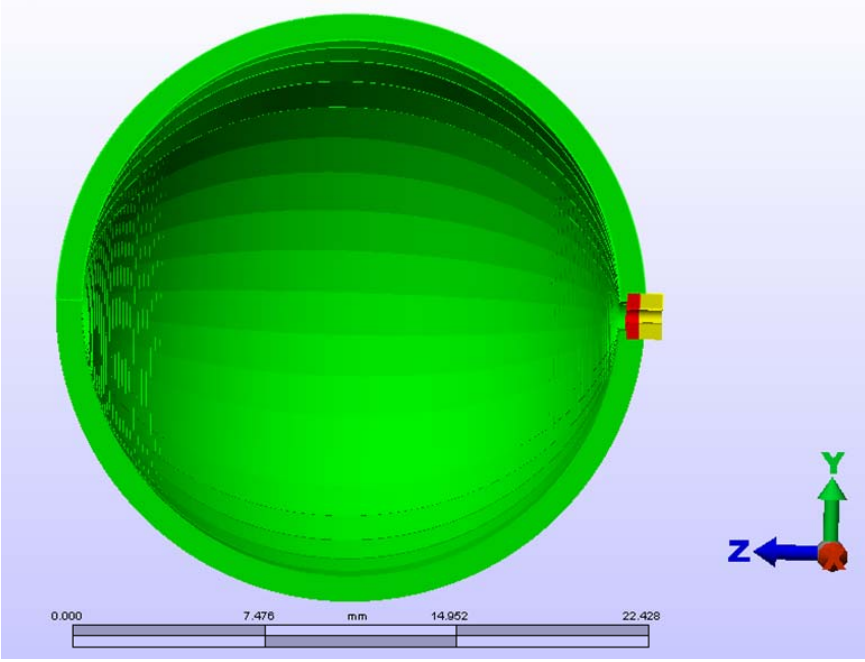

Figure 1. Full model of lamina cribosa (red) and optic nerve (yellow) region.

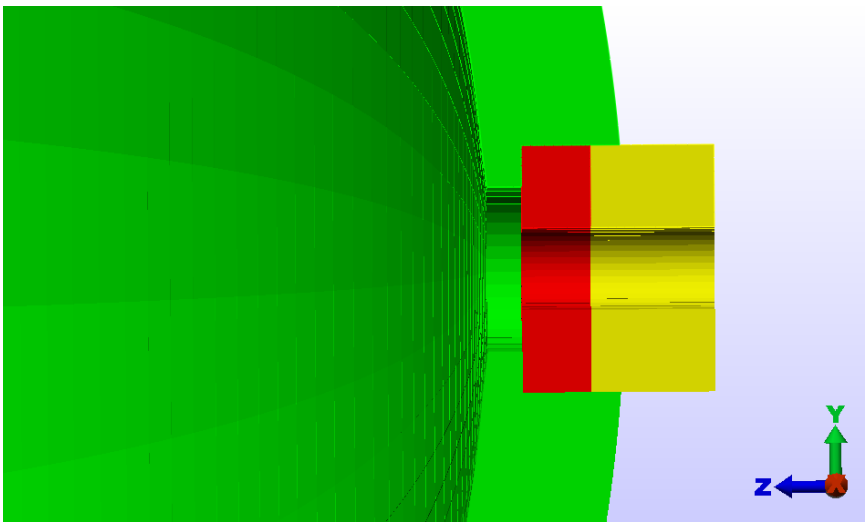

Figure 2. Enlarged view of lamina cribosa (red) and optic nerve (yellow) region

The half model of the eye was chosen to reduce the size of the model and it was sufficient to represent the boundary conditions which were used to model the incision in the RON surgical procedure. A 2-dimensional axisymmetric model could be developed but it would not include the option to use the cut area. The axisymmetric model was explored briefly since it is advantageous for modeling and computation time purposes. The 3-dimensional model that was developed was optimized to meet analysis needs and to compute results in a reasonable length of time.

3.0 MODEL DIMENSIONS

We assumed that the globe of the eye was a hemispherical shell with an inner diameter of 20 mm and an outer diameter of 22 mm (scleral thickness = 1 mm). The diameter of the optic nerve was assigned to be 1.5 mm and the central opening for the vein passing through the nerve was assumed to be 0.3 mm. The central venous lumen diameter was assumed to be 0.3 mm and the thickness of the lamina cribosa was set at 0.5 mm. The length of the optic nerve segment as modeled was 1.25 mm. The entire nerve has decreasing influence the further away it is from its insertion into the posterior globe. The optic cup diameter and depth were modeled at 0.9 mm and 0.25 mm, respectively. These dimensions are shown in figure 3.

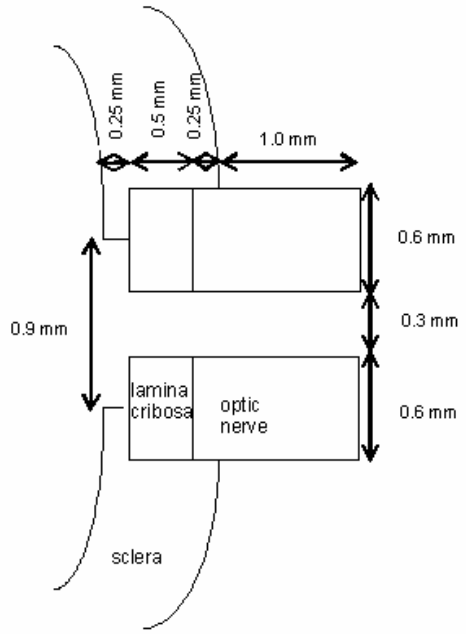

Figure 3. Model geometry of the optic nerve head

When the model was created, the three part assembly could be made in the finite element environment or a CAD (Computer Aided Drafting) environment. The finite element environment was chosen due to the assumptions made for creating the model and the desire to use a more structured mesh. A 2-dimensional sketch of the model was drawn in Algor software and then rotated into 3-dimensions. The 2-dimensional sketch was meshed using an automatic meshing routine. The automatic meshing routine was used in the 2-dimensional development so that refinement could be easily added. Refinement is discussed in further detail in the mesh convergence study. Once the 2-dimensional portion was modeled in the YZ plane, the entire section was rotated 180° about the Z axis. When the section was rotated, the option to join all of

the copies was activated. The join option then created the solid mesh as each copy was rotated. Twenty rotations were used over the entire model. This provided a three dimensional model which was reasonable in element count and thus would not be too expensive computationally to run on a desktop PC. The average analysis time was 9.72 minutes, and the number of elements in the model was 24,960.

4.0 BOUNDARY CONDITIONS

For the untreated eye model, symmetric boundary conditions were assigned to nodes in the plane of symmetry (y-z plane). In addition, to prevent rigid body motion, the leftmost node in the sclera on the plane of symmetry was constrained not to move in the y and z directions and the node to the right of this on the inside of the sclera was constrained in the y direction. To model the incision for RON surgery the constraint in the x direction is removed for the nodes in the area of the RON incision (Figure 4) on the plane of symmetry. In this way these nodes are free displace perpendicular to the plane of symmetry and hence separate from the tissue that is the mirror image forming an incision. All other interfaces between different tissues are bonded.

A linear static stress analysis was used for each case. Statically stable conditions were achieved by using symmetry conditions and an extra Y and Z constraint at the top of the sclera so that the model did not move out of plane. Figures 5 and 6 show the difference between the cut and uncut boundary conditions. Figure 5 shows that all of the symmetry conditions are still on the "cut" location while Figure 6 shows the nodes without boundary conditions.

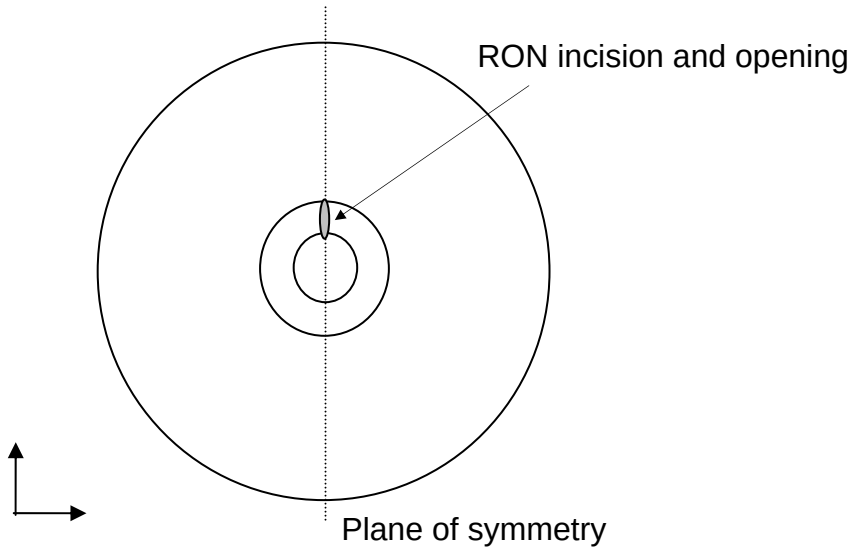

Figure 4. RON incision location

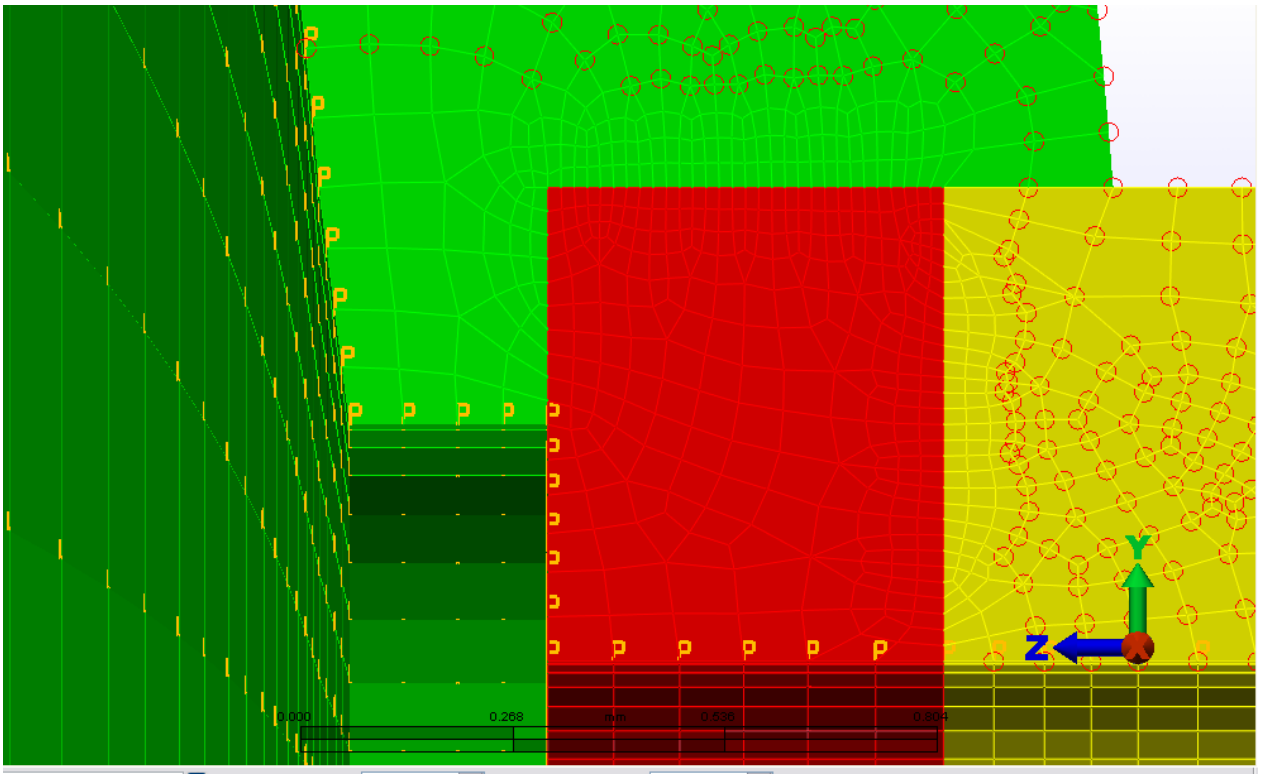

Figure 5. Model with cut conditions

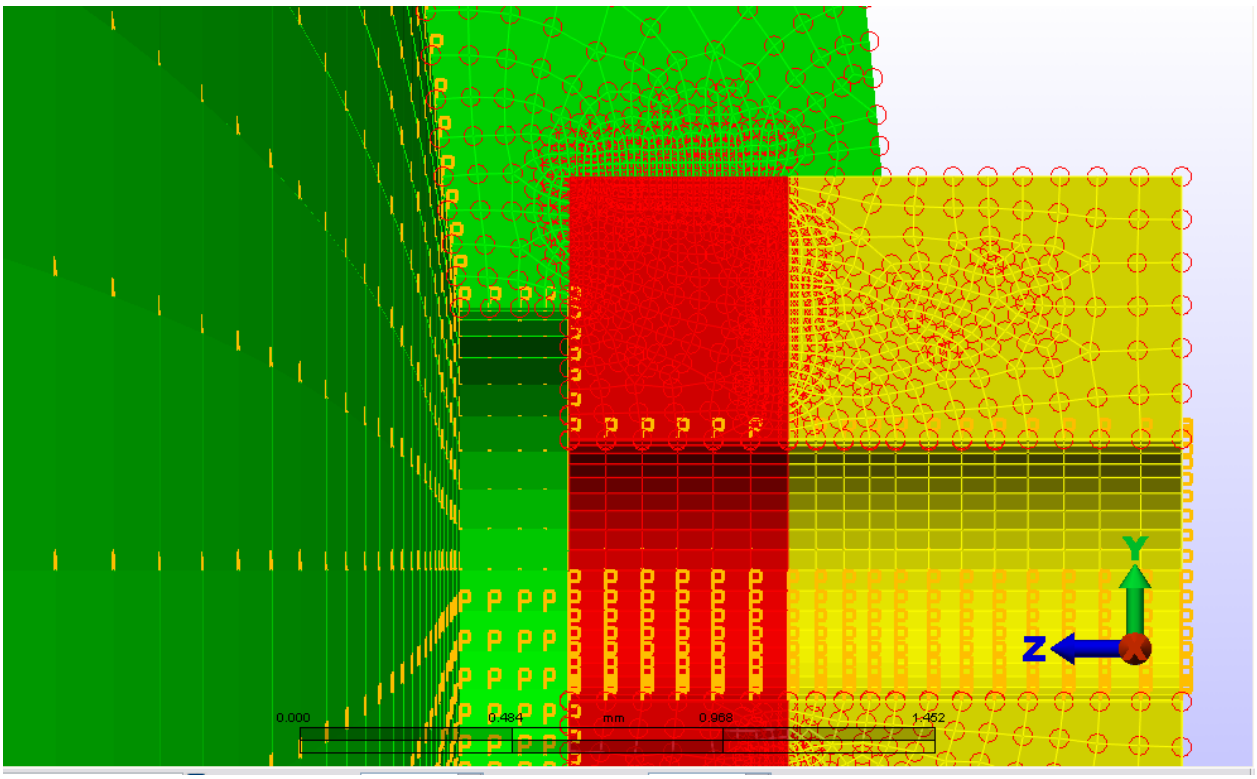

Figure 6. Model with uncut conditions

5.0 LOADS

An interocular pressure (IOP) was applied to all internal surfaces of the sclera and the surface of the lamina cribosa having a normal direction into the globe of the eye. A uniform venous pressure was applied to the internal surface of the optic nerve and lamina cribosa. The external surfaces of all tissues were free surfaces. The physiological ranges of values used for the IOP were 15, 25 and 35 mm Hg, while 50 and 75 mm Hg were used for the venous pressure.

Pressures are shown in the modeling environment in Figures 7 and 8. The yellow "P" symbol show graphically where the pressures are applied, and the red circles show boundary condition locations.

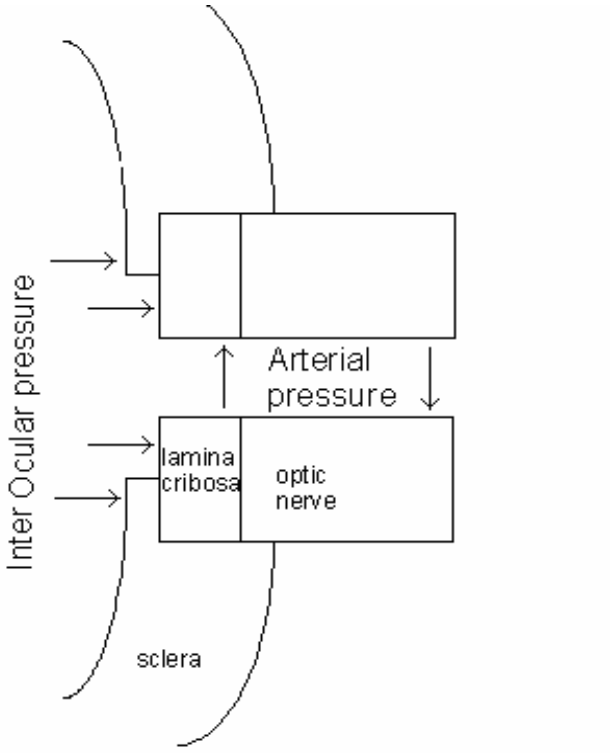

Figure 7. Loads applied to the model

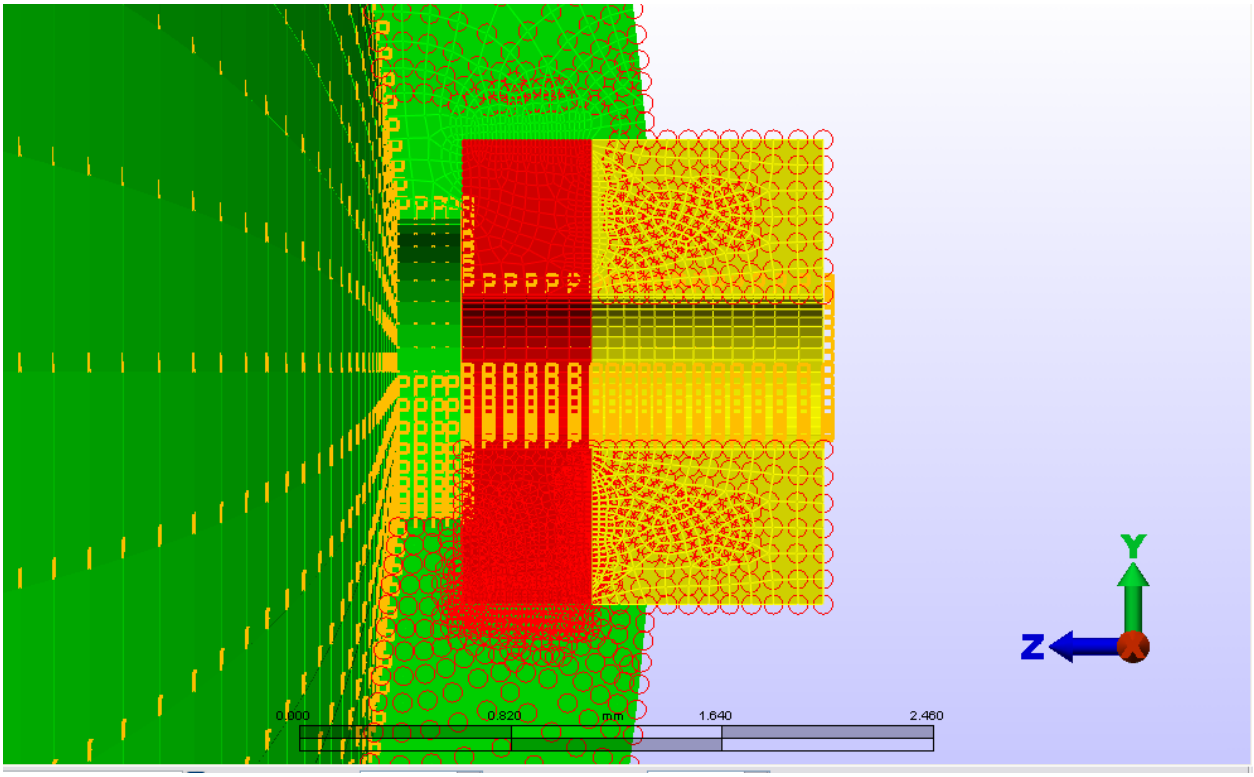

Figure 8. Zoomed view of the loads applied to the model

6.0 MATERIAL PROPERTIES

All tissues were assumed to be linearly elastic, isotropic and nearly incompressible with Poisson's ratio equal to 0.49. For scleral tissue the modulus of elasticity was taken to be E_s=2.5 MPa from testing done by Friberg and Lace [22]. There is uncertainty in the material properties of the lamina cribosa but the approximate mean value of the modulus of elasticity for human tissue is E_{lc}=0.25 MPa [25]. For the modulus of the optic nerve tissue there is a lack of information and two different values were chosen for the analysis. A stiff value for the neural tissue modulus was four times that of the sclera ($E_n = 4E_s$) while the compliant neural tissue had a modulus of one-tenth that of the sclera ($E_n = 0.1E_s$).

7.0 MESH CONVERGENCE STUDY

A mesh refinement study was done to evaluate the accuracy of the model. ALGOR V19 software (Algor Inc, Pittsburgh PA) was used to perform finite element analysis of the model. The analysis was done using the symmetric (non RON) conditions. Eight node hexahedral elements were used in the model. For the mesh refinement, the three parts of the mesh, the sclera, optic nerve and lamina cribosa were each meshed with the same number elements (in the 2-dimensions mesh) and three cases were examined 300, 650 and 1000 elements.

Since in this study the displacement is of interest rather than the stress, the maximum nodal displacement was calculated for each mesh. This occurred in the same location for all models, the inside upper edge of the cribiform plate. This quantity changed by less than 1% with each refinement, see Figure 9.

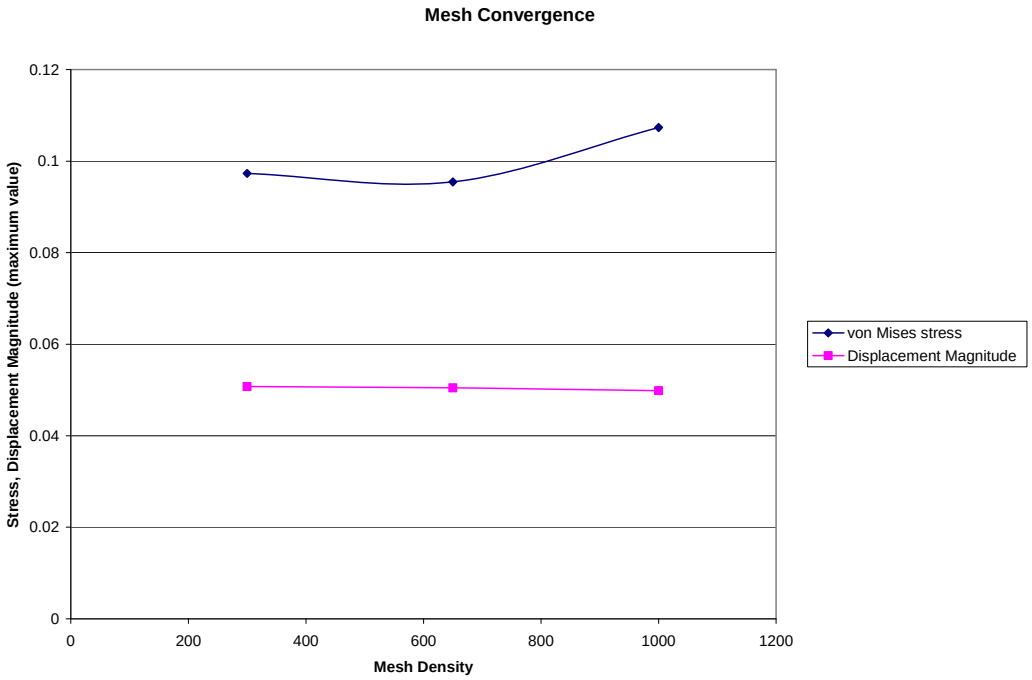

Figure 9. Mesh Convergence Study results

The stress values show more variation. The variation was considered to be from the mesh size and refinement between parts in the model. Figures 10, 11 and 12 show the maximum stress location for the different mesh densities which also indicated that the mesh needs to be locally refined. The maximum stress location is marked in each figure with a red "Max" flag.

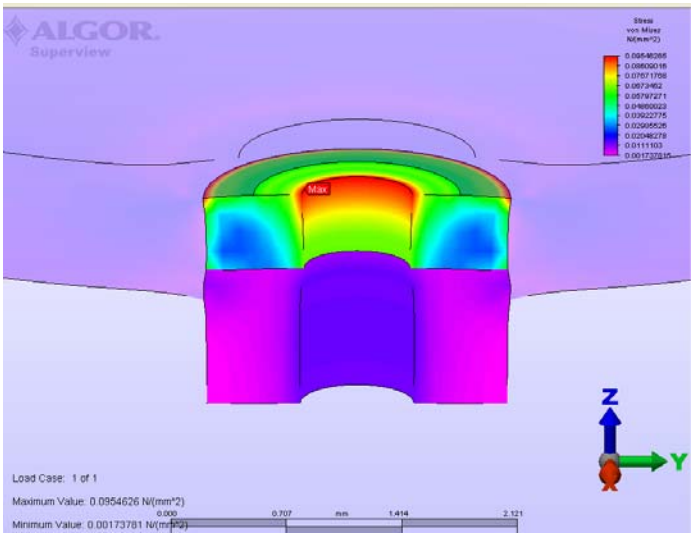

Figure 10. 300 element mesh density model with maximum stress location

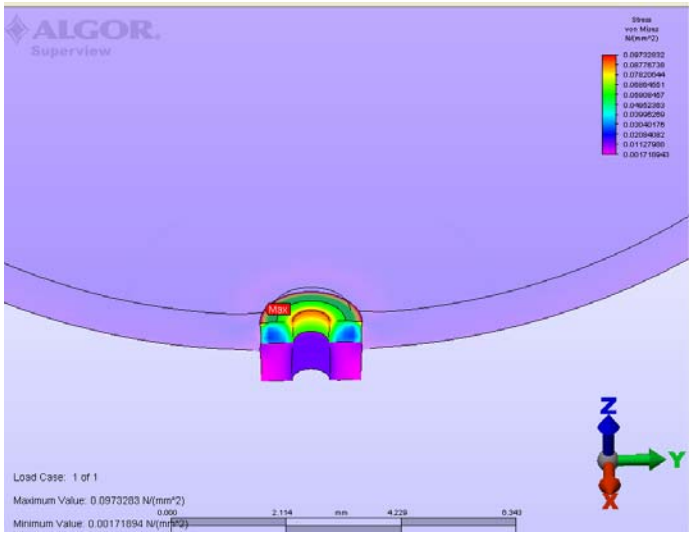

Figure 11. 650 element mesh density model with maximum stress location

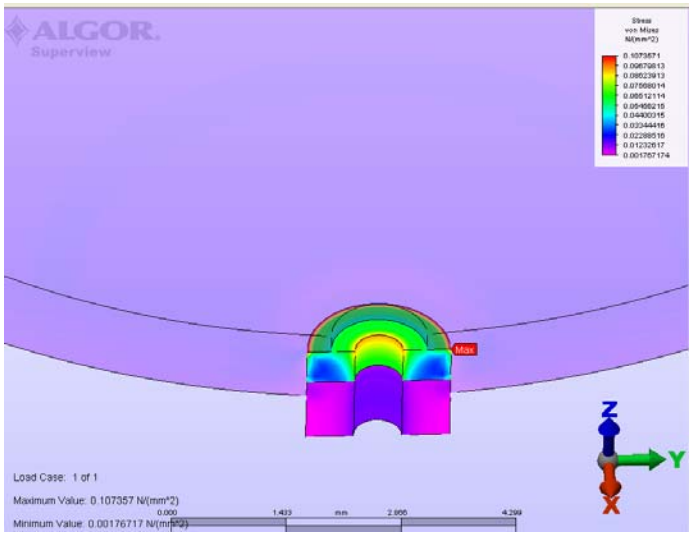

Figure 12. 1000 element mesh density model with maximum stress location

The finest mesh density model was used for further local refinement. It was determined that there needed to be at least three elements through the thickness of the sclera. There should

be at least three elements because the interocular pressure is applied directly to the sclera inside edge. Figures 13 and 14 show refinement of the sclera part. Black dots indicate where the mesh refinement was used. Further local refinement was used along the edges between the cribriform plate and optic nerve areas that touch the sclera, see Figure 15. The edge of the cribriform plate had 30 mesh divisions specified along the vertical edge and 10 divisions along the top. The mesh divisions are specified on the coincident lines between the cribiform plate and the optic nerve (or the cribiform plate and sclera). This ensured that the mesh would match between each part. This mesh was determined to be the best configuration based on the Y displacement results and mesh quality. Figure 16 shows the analysis results and the Y displacements. The Y displacement values from the results legend box are symmetric. Figure 17 shows the stress distribution also is symmetric. This mesh was then used for the various case studies where pressures and material properties were varied. The final three-dimensional mesh had 24,960 elements.

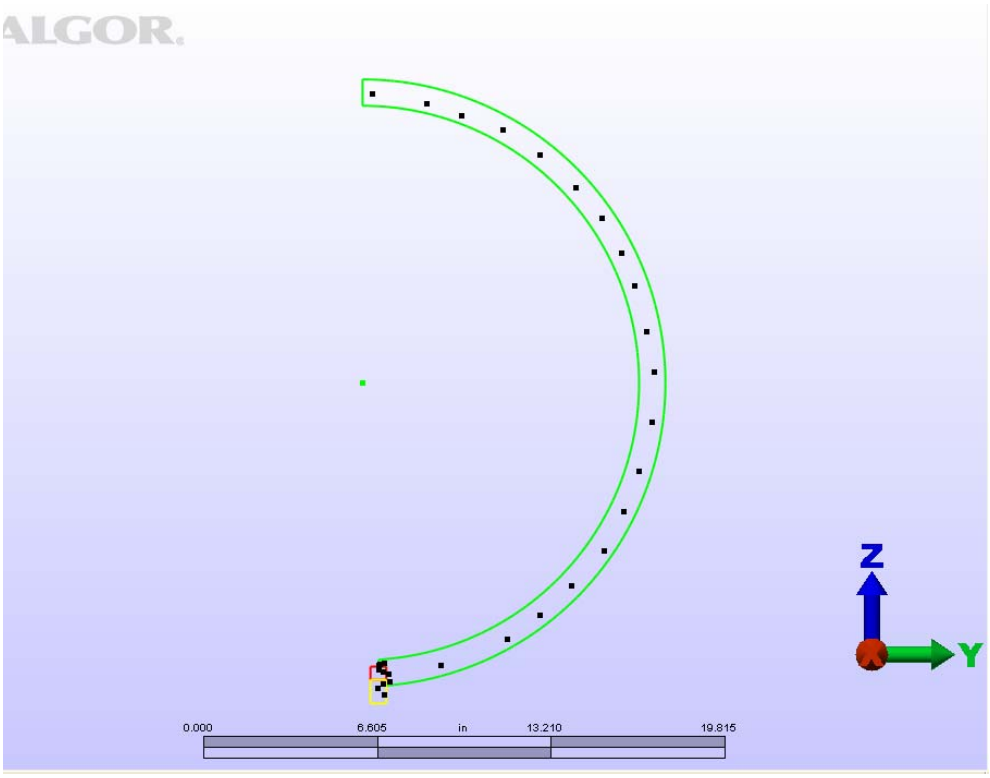

Figure 13. Mesh refinement points in 2-dimensional model

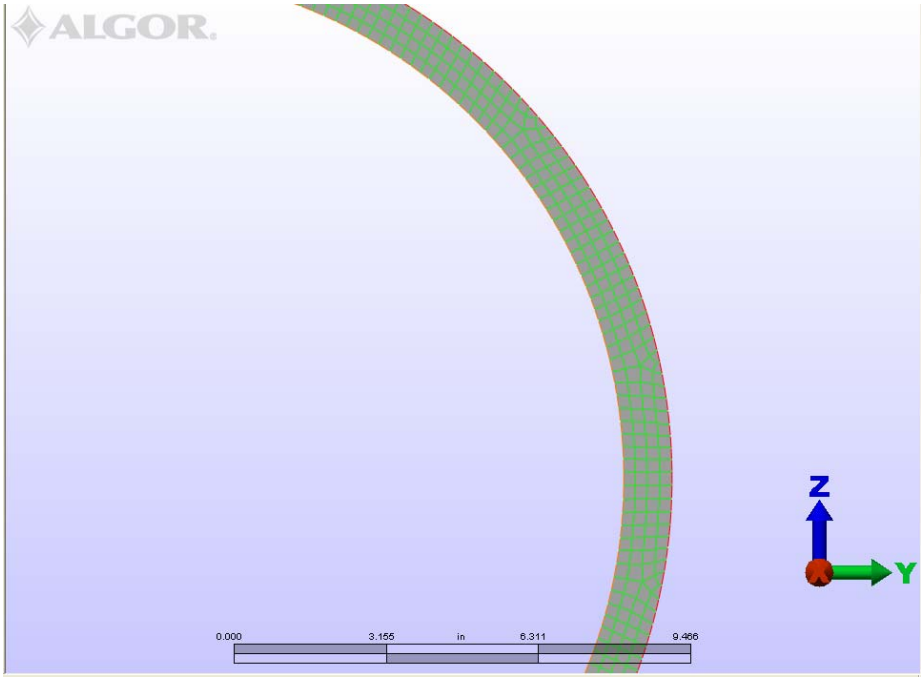

Figure 14. Automatic mesh with 4 elements through the thickness

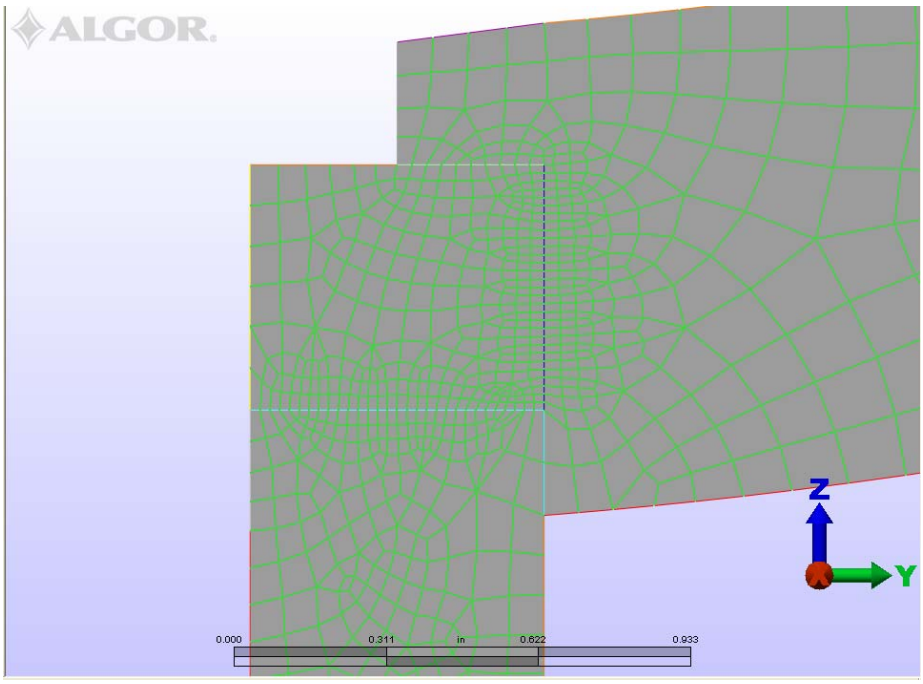

Figure 15. Model with edge refinement

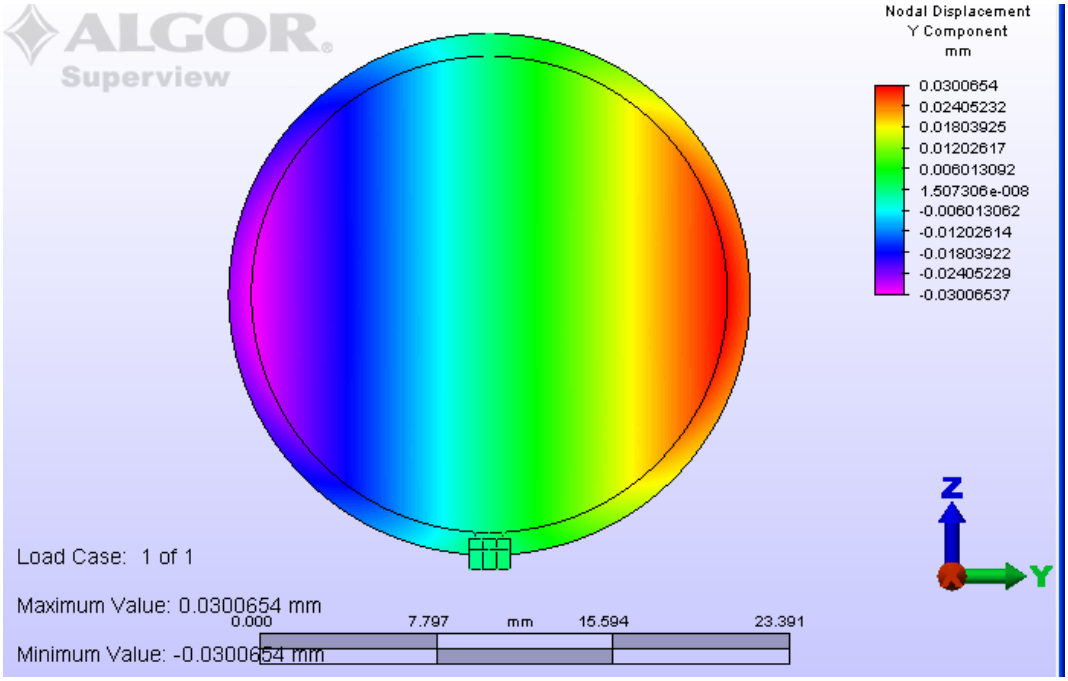

Figure 16. Displacement results of mesh convergence study

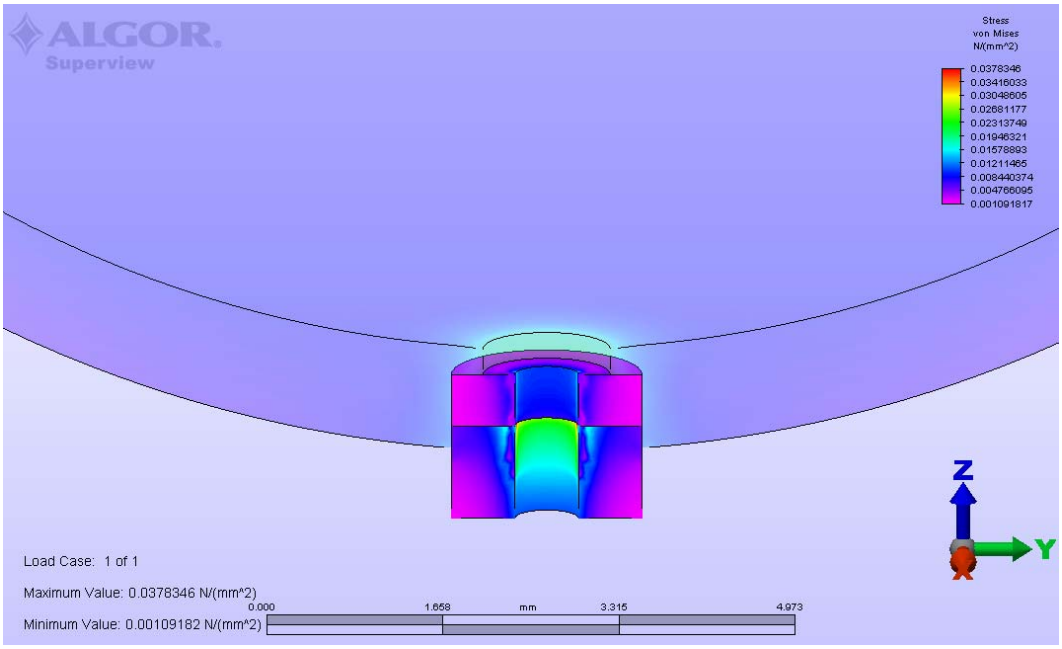

Figure 17. Stress results of mesh convergence study

8.0 ANALYSIS PARAMETERS

Using the different material properties and pressures, several cases were set up for analysis. Table 1 shows the case sets that were analyzed. Each case was run with the RON incison and no incision conditions. This made twenty-four total cases that were analyzed. Ron incision cases included the removed symmetry boundary conditions while no incision cases included the symmetry conditions in the incision region.

Table 1. Loads and material properties for analysis

Poissons Ratio	Sclera Modulus	Cribiform Plate Modulus	Optic Nerve Modulus	Inter Ocular Pressure	Arterial Pressure
.49	2.5 MPa	0.25 MPa	10 MPa	10 mm Hg	50 mm Hg
			0.25 MPa	25 mm Hg	75 mm Hg
				35 mm Hg	

The sparse solver was used for analysis. The analysis took 9.7 minutes to solve for the displacements and an additional 0.6 minutes to solve for the stresses. The RON incision case included 6,708,249 entries in the stiffness matrix from 86,164 equations. The no incision case included 6,659,296 entries in the stiffness matrix from 85,597 equations. The difference in equations and matrix entries comes from the boundary conditions in the incision area. Appendix A includes the log file for Case 1 with the incision conditions. Appendix B includes the

summary file for Case 1 with the incision conditions. Appendix C includes the log file for Case 1 with the no incision conditions. Appendix D includes the summary file for Case 1 with the no incision conditions.

9.0 RESULTS

9.1 NODES USED FOR RESULTS

The model has been analyzed with and without the RON procedure to study the effect of the procedure on the size of the central lumen of the optic canal. Without the RON procedure, there is no difference in the diameter of the central lumen in the x and y directions because of symmetry. However, with RON, the diameter in these two directions is not the same. For this reason the displacements were taken at the nodes shown in Figure 18. The Y displacement were taken at the top and bottom of the right and left side of the cribiform plate. The X displacement was taken at the top of the cribiform plate and the bottom of the optic nerve. Figure 18 shows marked locations. For the model without the RON incision the Y displacements right and left hand side of the cribiform plate would have the same magnitude but be opposite in sign because of the symmetry of the problem.

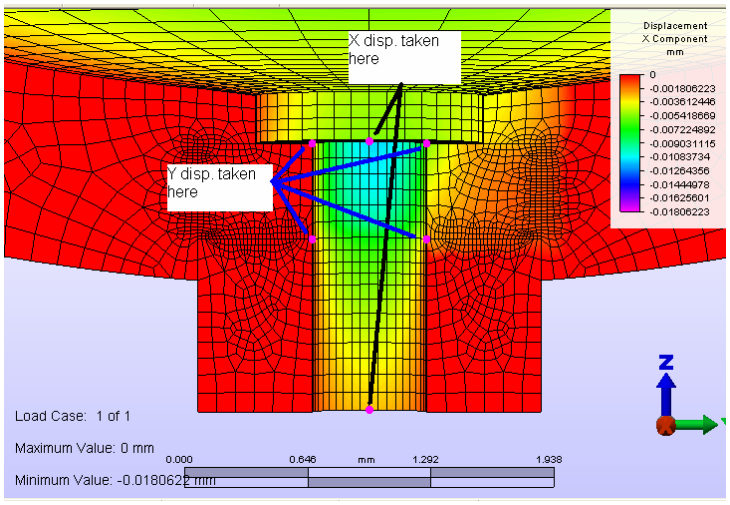

Figure 18. Locations of displacement values

The nodes chosen to be monitored for X and Y displacement values were the same for all cases. To ensure that the same nodes were always chosen, a script was created to record the displacement values. The script took advantage of exposed functions in the Algor interface. The functions used in the ALGOR interface were from the results environment. The functions used in this script pick a node, find the displacement value, and then record this value to a text file. The input for the script only required a list of nodes, and these nodes were the locations shown above in Figure 18. The script is included in Appendix E.

9.2 RESULTS OVERVIEW

These graphs give the central lumen diameter with RON normalized by to the central lumen without RON as a function of the interocular pressure. The diameter of the central lumen is defined as the distance between opposing in the channel. The four lines in the graph

correspond to different values of nerve elastic modulus ($E_n = 4E_s$ and $E_n = 0.1E_s$ and venous pressure (50 and 75 mm Hg).

Figures 19 and 20 give this data for the full model (sclera, cribiform plate and optic nerve). These graphs show the ratio of central lumen diameter with RON to central lumen diameter without RON as a function of interocular pressure for different nerve moduli and venous pressures. These figures are for the upper nodes shown in Figure 18 above. Figures 21 and 22 show the deformation in the area of the cribiform plate for the RON incision and intact full model. Figures 21 and 22 are the results of the case where $E_n/E_s=4$, the venous pressure is 50 mm Hg, and the interocular pressure is 10 mm Hg. Note the circumferential symmetry in Figure 21.

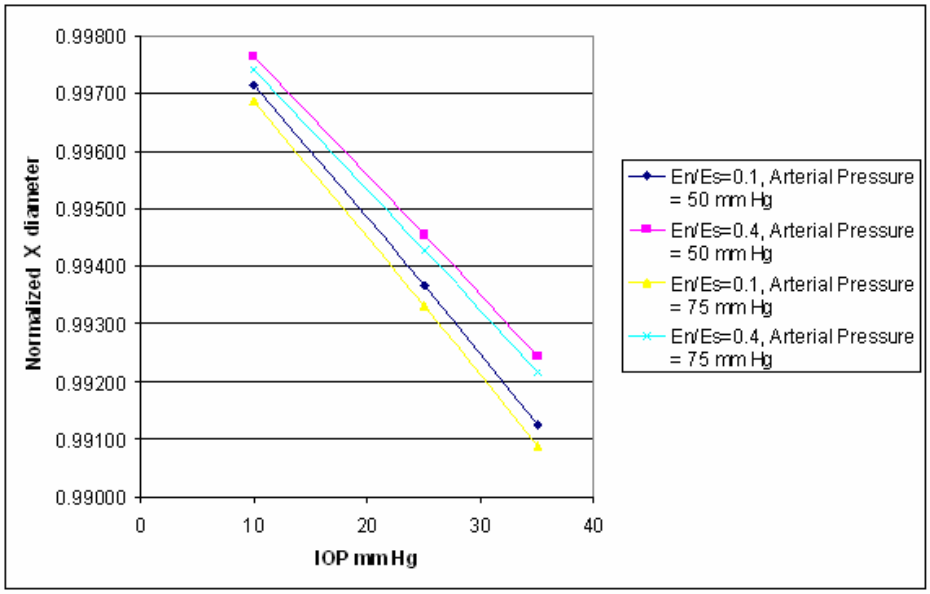

Figure 19. Normalized X direction diameter

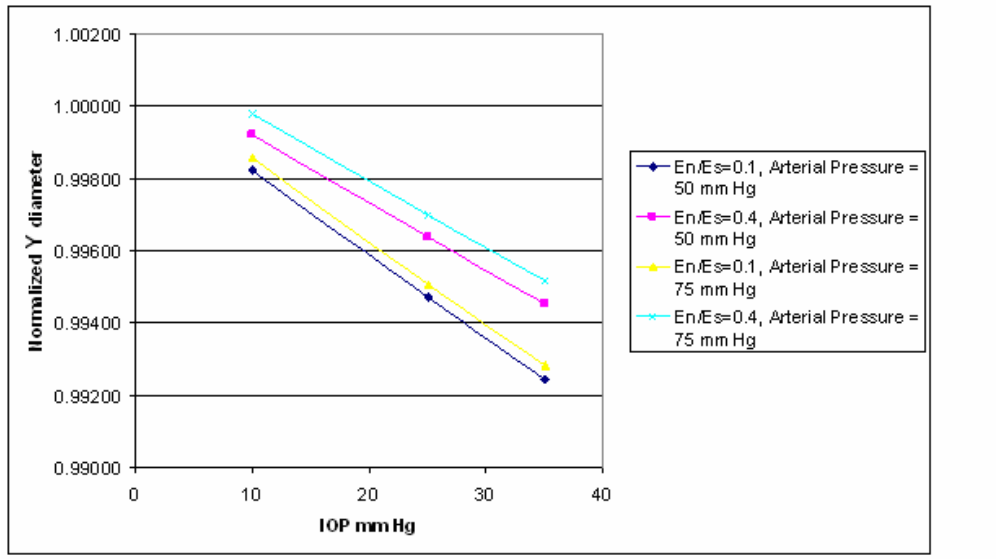

Figure 20. Normalized Y direction diameter

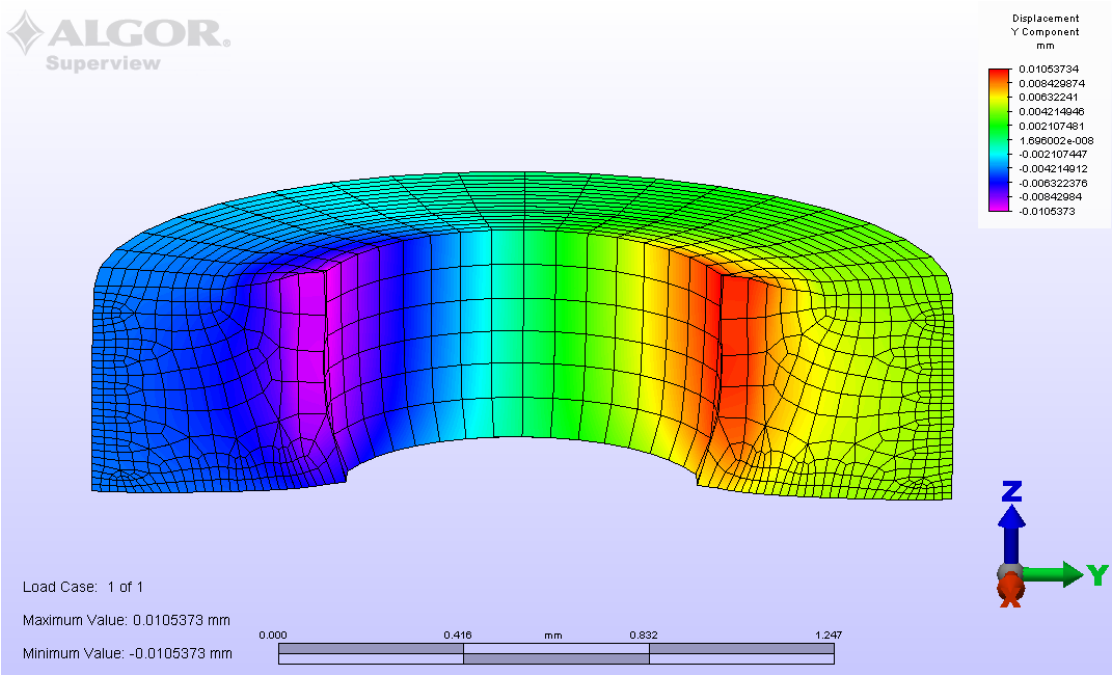

Figure 21. Plot of the deformed geometry of the model with the RON incisioin

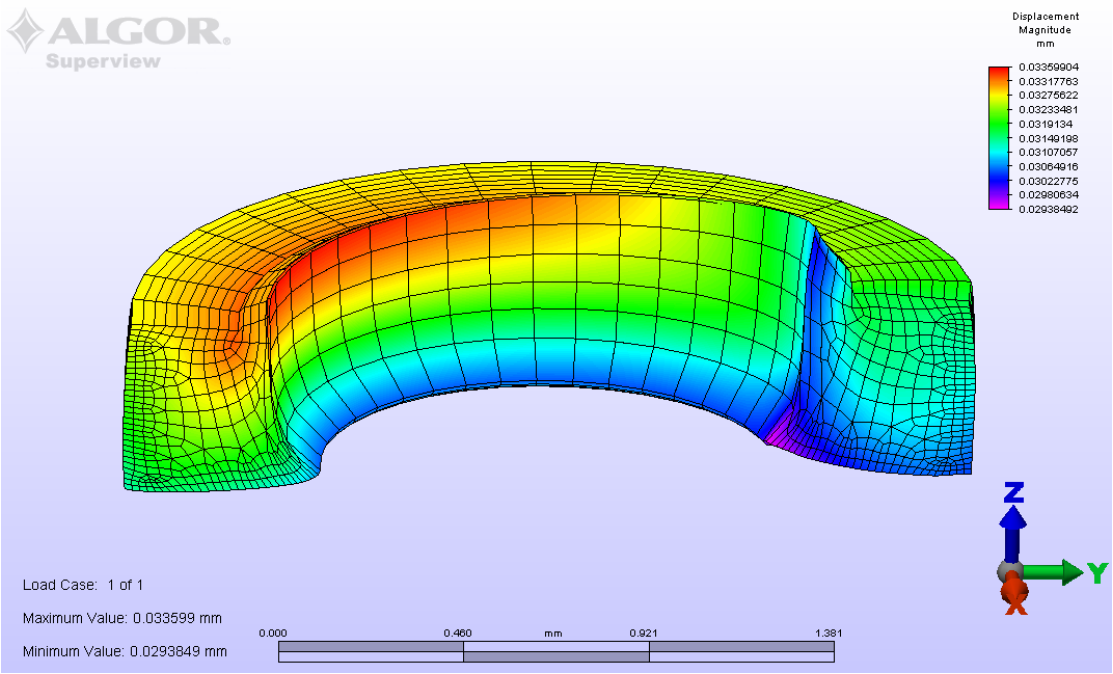

Figure 22. Plot of the deformed geometry of the model with the RON incision

9.3 EFFECTS OF MATERIAL PROPERTIES AND INTEROCULAR AND VENOUS PRESSURES

The following figures include the results summary of the twelve cases analyzed in the incision and non-incision conditions. In the legend box, dashed lines are for the incision cases and solid lines are for the non-incision cases. Each graph set shows the displacements of the nodes along the z-direction on the left hand side (LHS), right hand side (RHS) or center results of observed nodes in the central lumen. Red lines (solid and dashed) indicate cases where the nerve elastic modulus was $E_n = 4E_s$ and green lines (solid and dashed) indicate the nerve modulus was $E_n = 0.1E_s$. The chart title indicates the venous pressure (50 or 75 mm Hg) and the interocular pressure (10 mm Hg, 25 mm Hg or 35 mm Hg). The vertical axis is the Z coordinate

of the node being observed, and the horizontal axis is the Y (or X) displacement value of the observed node.

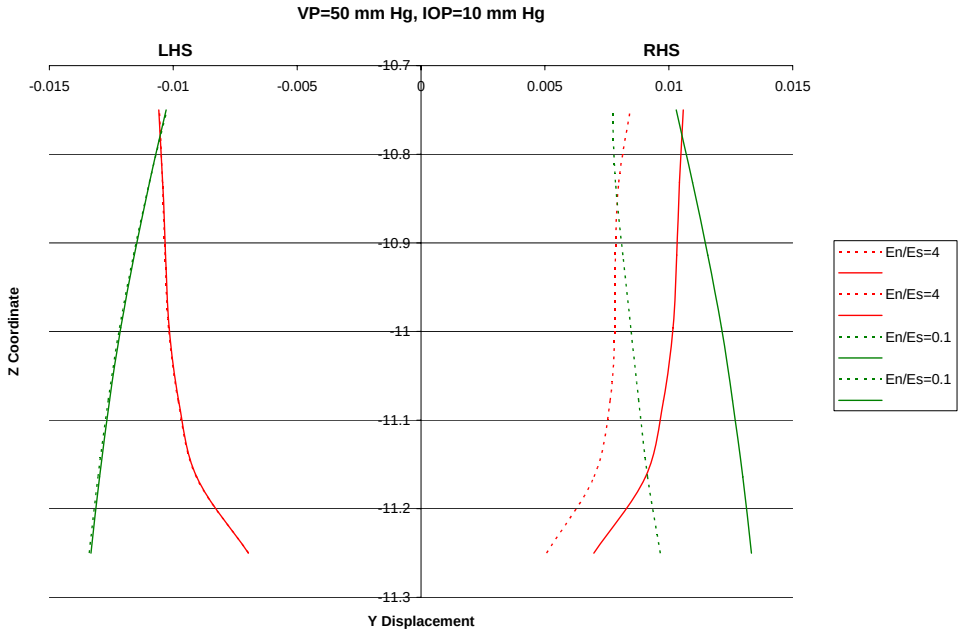

Figure 23. Full model results of VP=50 mm Hg, IOP=10 mm Hg Left Hand side and Right Hand side cases

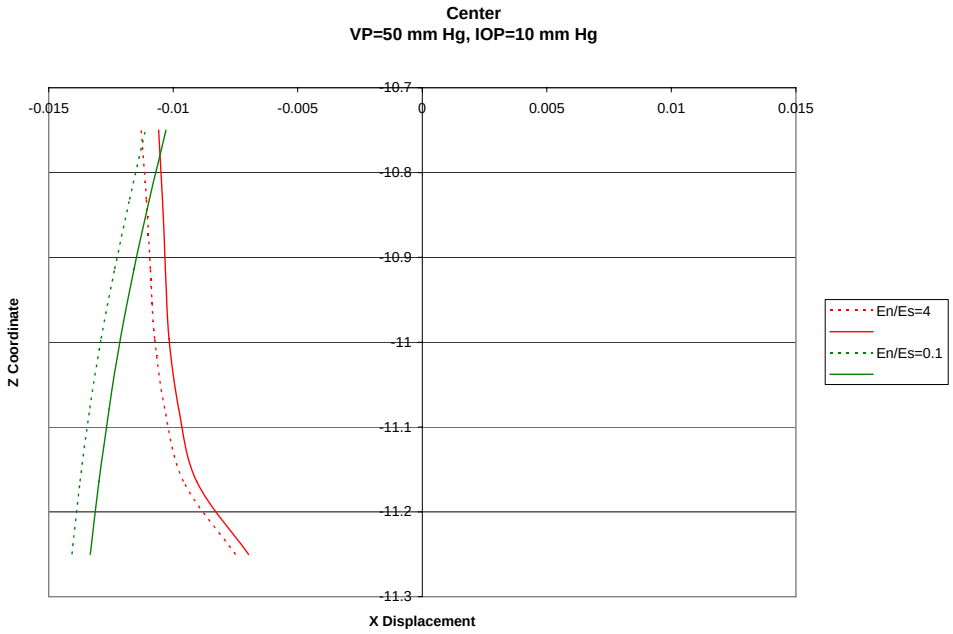

Figure 24. Full model results of VP=50 mm Hg, IOP=10 mm Hg Center cases

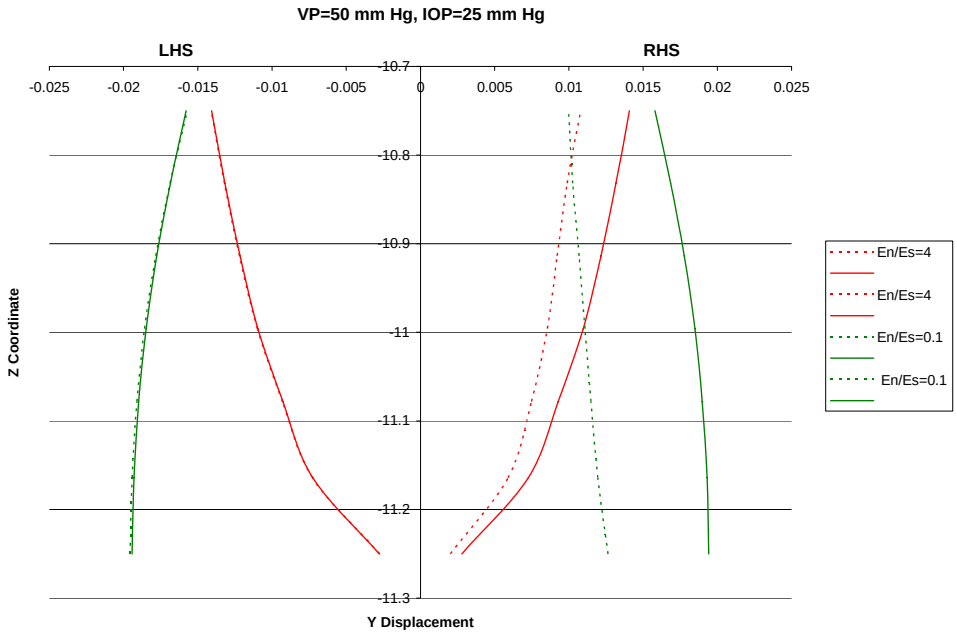

Figure 25. Full model results of VP=50 mm Hg, IOP=25 mm Hg Left Hand side and Right Hand side cases

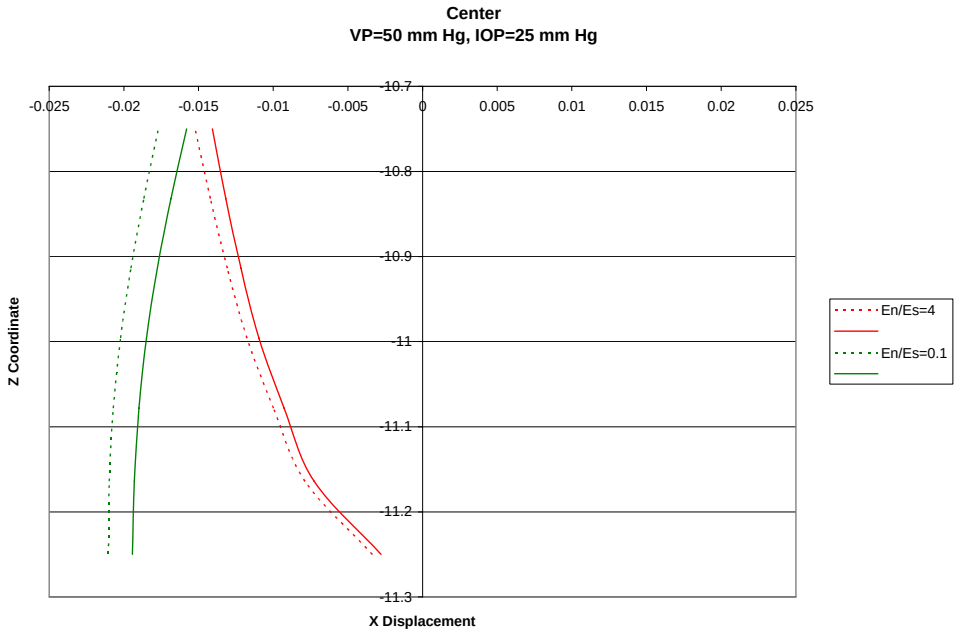

Figure 26. Full model results of VP=50 mm Hg, IOP=25 mm Hg Center cases

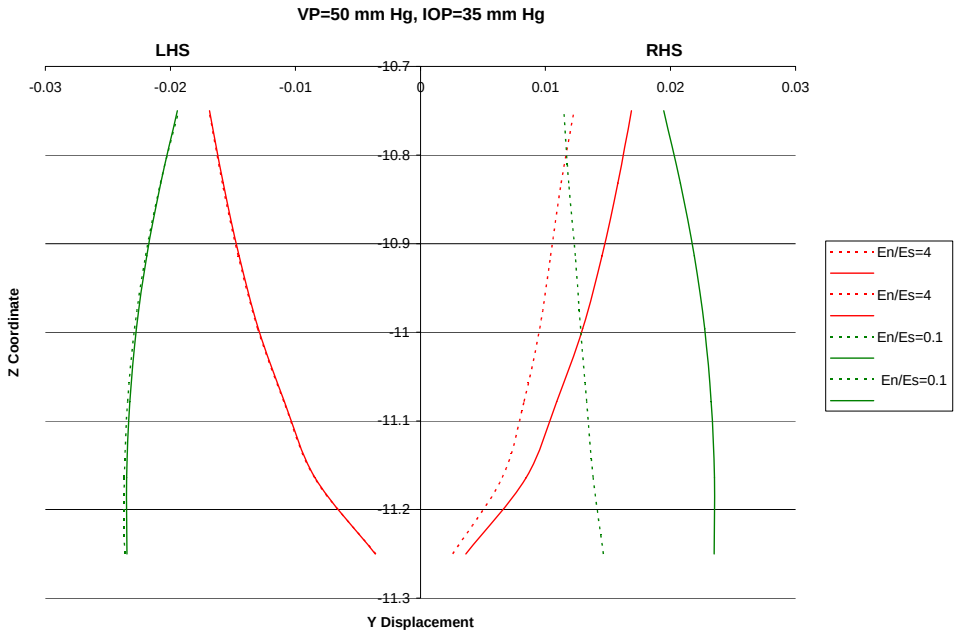

Figure 27. Full model results of VP=50 mm Hg, IOP=35 mm Hg Left Hand side and Right Hand side cases

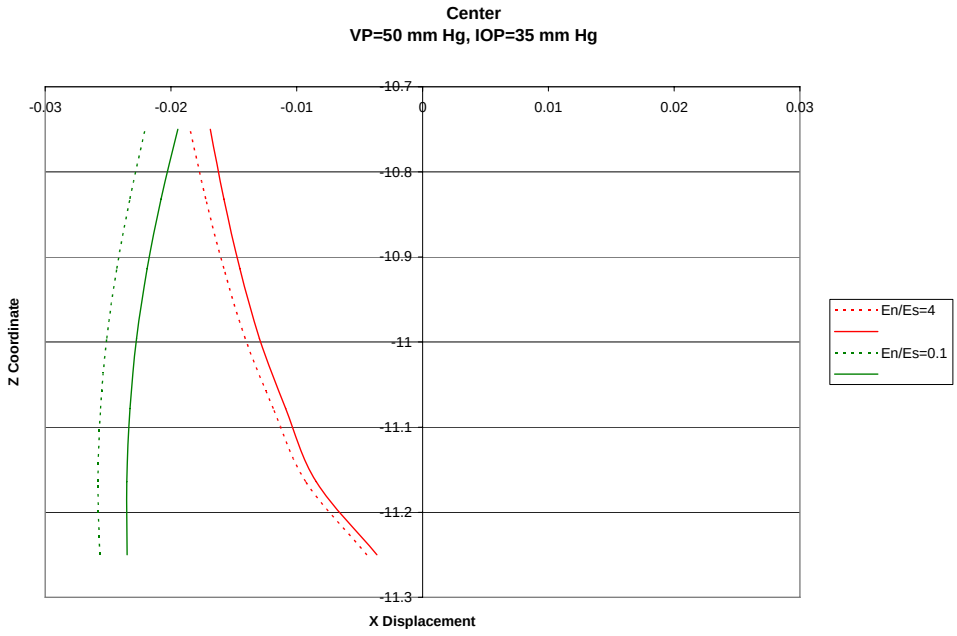

Figure 28. Full model results of VP=50 mm Hg, IOP=35 mm Hg Center cases

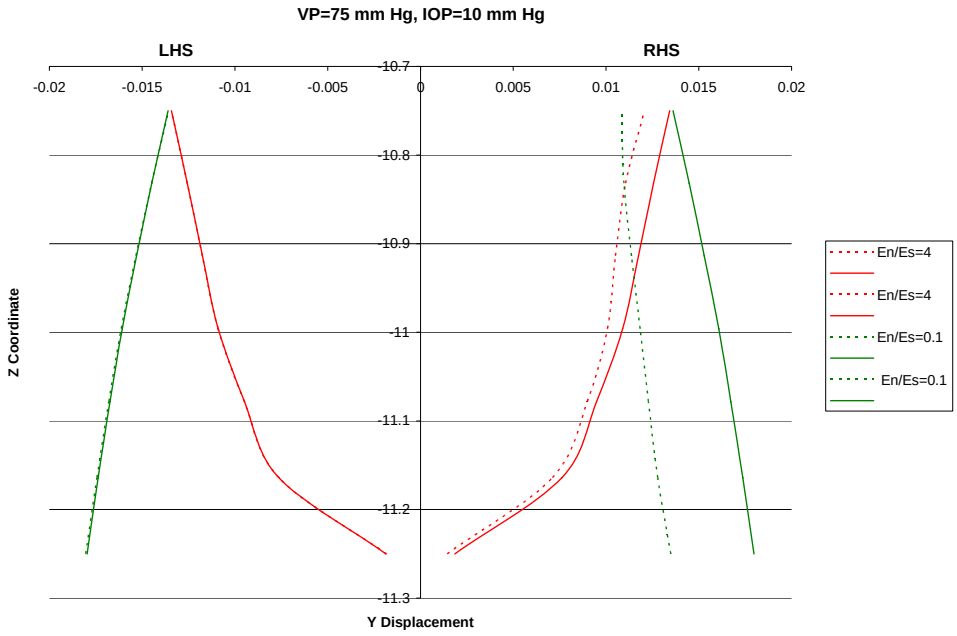

Figure 29. Full model results of VP=75 mm Hg, IOP=10 mm Hg Left Hand side and Right Hand side cases

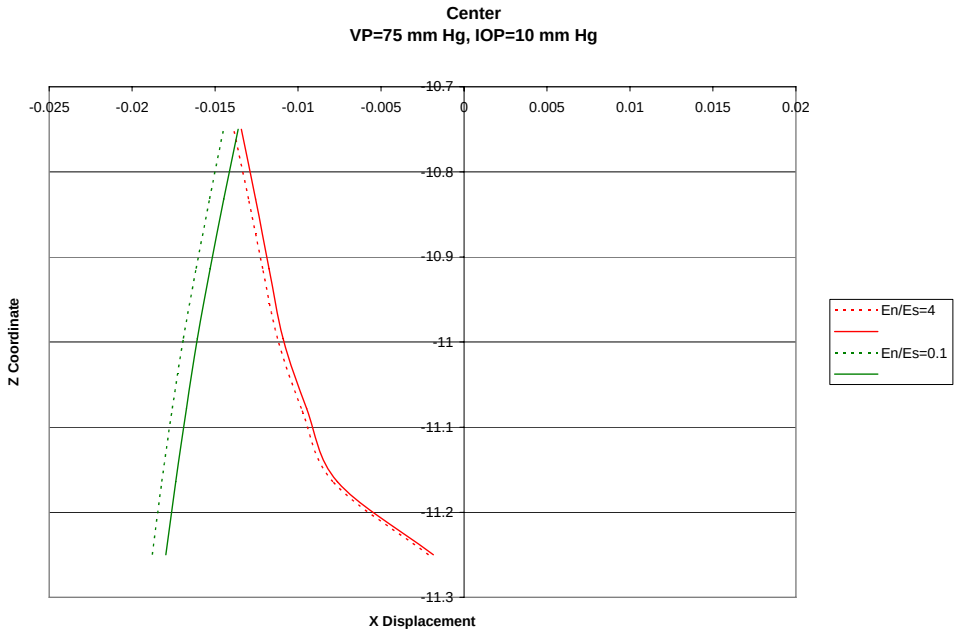

Figure 30. Full model results of VP=75 mm Hg, IOP=10 mm Hg Center cases

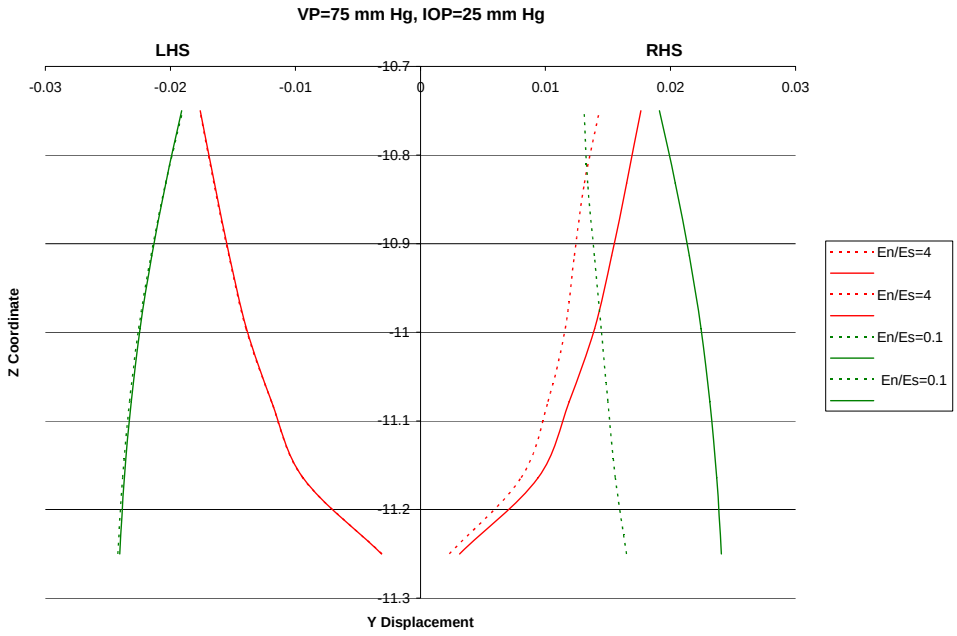

Figure 31. Full model results of VP=75 mm Hg, IOP=25 mm Hg Left Hand side and Right Hand side cases

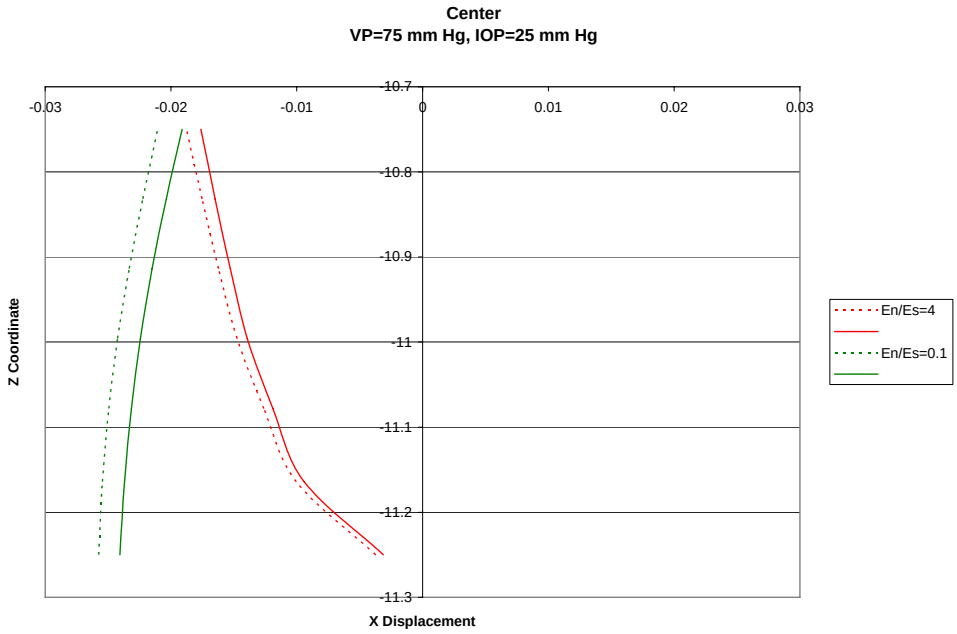

Figure 32. Full model results of VP=75 mm Hg, IOP=25 mm Hg Center cases

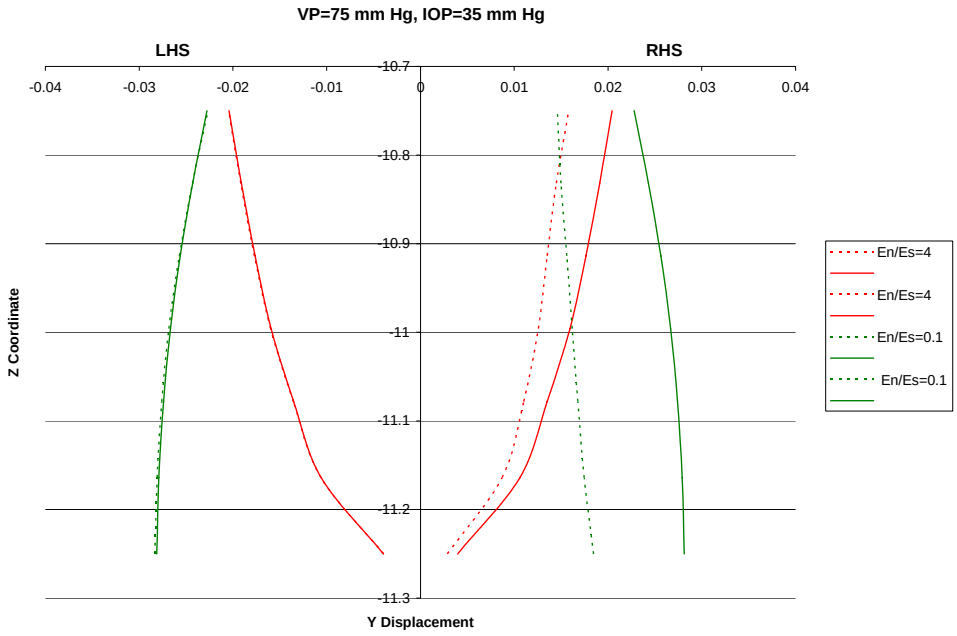

Figure 33. Full model results of VP=75 mm Hg, IOP=35 mm Hg Left Hand side and Right Hand side cases

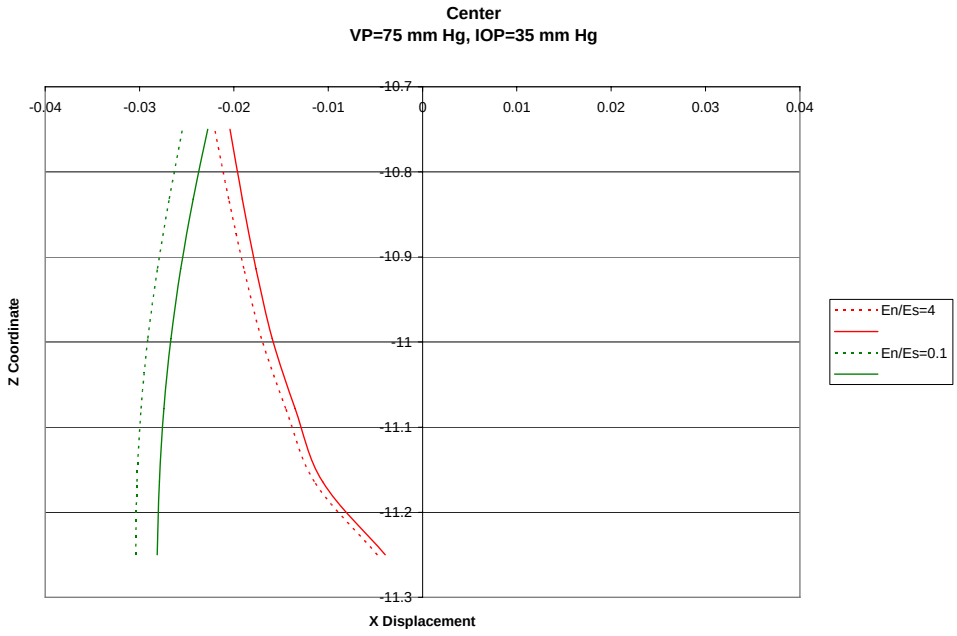

Figure 34. Full model results of VP=75 mm Hg, IOP=35 mm Hg Center cases

From these graphs there are conclusions that can be drawn about the effect of the RON incision on the deformation in the central lumen concerning the Y displacements and maximum or minimum openings of the central lumen diameter. Changing the venous pressure or interocular pressure resulted in a different magnitude for the Y displacement values, but it did not change the trend of the lines for right hand side, left hand side or center observations. The left hand side deformation, for all cases, showed the largest displacement in the incision cases and E_n/E_s=0.1. The right hand side deformation, for all cases, showed the largest displacement for the non-incision cases and E_n/E_s=0.1. For E_n/E_s=0.1 and E_n/E_s=4, and the left hand side and right hand side, the largest Y displacement occurs at Z coordinates of -11 to -11.1 millimeters for the nonincision cases. For E_n/E_s=4 and the left hand side and right hand side, the largest Y displacements occur at Z coordinates of -11.1 to -11.2 millimeters for incision cases. For E_n/E_s=0.1 and the left hand side and right hand side, the largest Y displacement occurs at the furthest distance down the vein in the Z direction.

The smallest Y displacement occurred in the VP=50 mm Hg , IOP=10 mm Hg cases on the right hand side for E_n/E_s=0.1, see Figure 23. The largest Y displacement occurred in the VP=75 mm Hg, IOP=35 mm Hg cases on the left hand side for both E_n/E_s=0.1 and E_n/E_s=4, Figure 33. These results also support the previous statement that changing the pressure values changed only the magnitude of the Y displacement values. The largest pressure values for venous and interocular pressures resulted in the largest displacements, while the smallest pressure cases provided the smallest displacement values.

The largest change in right hand side, top diameter values between incision and non-incision cases occurred in VP=50 mm Hg, IOP=35 mm Hg cases, Figure 27. The smallest change in right hand side, top diameter values between incision and non-incision cases occurred in VP=75 mm Hg, IOP=10 mm Hg cases, Figure 29.

The smallest center diameter Y displacement occurred in VP=50 mm Hg, IOP=10 mm Hg. The largest center diameter Y displacement occurred in VP=75 mm Hg, IOP=35 mm Hg. Though values in VP=50 mm Hg, IOP=35 mm Hg were very close to the Y displacements in the largest center diameter Y displacement case of VP=75 mm Hg, IOP=35 mm Hg.

Similar to the Y displacement discussion, changing the venous pressure or interocular pressure resulted in a different magnitude for the X displacement values, but it did not change the trend of the lines for center observations.

The smallest X displacement occurred for E_n/E_s=0.1 and E_n/E_s=4 in the VP=50 mm Hg, IOP=10 mm Hg case, Figure 24. The largest X displacement occurred for E_n/E_s=0.1 and E_n/E_s=4 in the VP=75 mm Hg, IOP=35 mm Hg case, Figure 34. For E_n/E_s=0.1 and all cases, the smallest X displacement occurred at the smallest Z coordinate and then the X displacement value increases down the length of the Z axis. The largest X displacement then occurs at the largest Z coordinate for E_n/E_s=0.1 cases. For all E_n/E_s=4 cases, the largest X displacement occurs at the largest Z coordinate, the X displacement values then decrease as the Z coordinates increase.

APPENDIX A

LOG FILE FOR CUT CASE 1

ALGOR (R) Static Stress with Linear Material Models

Version 19.00-WIN 20-DEC-2005

29489 3 1 0 0 0

**** Linear stress analysis

**** Memory Dynamically Allocated = 523768 KB

Options executed are:

NOMIN

STRAIN

SPARSE

SUPCNF

SUPELM

SUPNOD

REAC

ENOR

```
    processing ...

**** OPENING TEMPORARY FILES
    NDYN = 0

                DATE: JANUARY 17, 2006
                TIME: 02:20 PM
           INPUT MODEL: E:\Pitt\THESIS\01172006\CUT\Mesh convergence_fine

         PROGRAM VERSION: 19000002
         alg.dll VERSION: 19000002
      agsdb_ar.dll VERSION: 18000000
     algconfig.dll VERSION: 19000000
      algsolve.exe VERSION: 19000000
      amgsolve.exe VERSION: 03300000

**** BEGIN NODAL DATA INPUT
    29489 NODES

**** END   NODAL DATA INPUT
**** BEGIN TYPE-8 data INPUT
    PART 1 CONTAINING 15280 ELEMENTS
       13000 (85.%) elements
       12000 (78.%) elements
       11000 (72.%) elements
       10000 (65.%) elements
```

9000 (59.%) elements

8000 (52.%) elements

7000 (46.%) elements

6000 (39.%) elements

5000 (33.%) elements

4000 (26.%) elements

3000 (20.%) elements

2000 (13.%) elements

1000 (7.%) elements

0 (0.%) elements

**** end TYPE-8 data INPUT

**** BEGIN TYPE-8 data INPUT

PART 2 CONTAINING 5620 ELEMENTS

3000 (53.%) elements

2000 (35.%) elements

1000 (18.%) elements

0 (0.%) elements

**** end TYPE-8 data INPUT

**** BEGIN TYPE-8 data INPUT

PART 3 CONTAINING 4060 ELEMENTS

2000 (49.%) elements

1000 (25.%) elements

0 (0.%) elements

**** end TYPE-8 data INPUT

**** Hard disk file size information for processor:

Available hard disk space on current drive = 7301.895 megabytes

**** BEGIN LOAD INPUT

Gravity direction vector = 0.0000E+00 0.0000E+00 -1.0000E+00

One load case in 43 blocks.

Load factor = 1.00E+00 in the 1st basket in load case 1

**** END LOAD INPUT

**** Invoking Sparse Solver ...

**** Symbolic Assembling Using the Row-Hits Matrix Profile ...

**** Assembled in One Block.

**** Real Sparse Matrix Assembly ...

in the upper off-diagonal matrix:

number of entries in the profile = 6708249

number of symbolic nonzero entries= 3145239

number of real nonzero entries = 3144927

**** Sparse Matrix Assembled in One Block

**** Load case 1

**** Sparse Matrix Factorization ...

**** Sparse Matrix Solving ...

**** End Sparse Solver Solution

**** BEGIN DISPLACEMENT OUTPUT

**** PRINT OF DISPLACEMENT OUTPUT SUPPRESSED

**** END   DISPLACEMENT OUTPUT

**** BEGINNING REACTION COMPUTATIONS

**** LOADCASES REMAINING   1

**** BLOCKS REMAINING   1

**** GROUPS REMAINING   3

**** GROUP USED--ELEMENT/GLOBAL CONTRIBUTIONS

15280 ELEMENTS

15280 ELEMENTS REMAINING

15000 ELEMENTS REMAINING

14000 ELEMENTS REMAINING

13000 ELEMENTS REMAINING

12000 ELEMENTS REMAINING

11000 ELEMENTS REMAINING

10000 ELEMENTS REMAINING

9000 ELEMENTS REMAINING

8000 ELEMENTS REMAINING

7000 ELEMENTS REMAINING

6000 ELEMENTS REMAINING

5000 ELEMENTS REMAINING

4000 ELEMENTS REMAINING

3000 ELEMENTS REMAINING

2000 ELEMENTS REMAINING

1000 ELEMENTS REMAINING

**** GROUPS REMAINING   2

**** GROUP USED--ELEMENT/GLOBAL CONTRIBUTIONS

5620 ELEMENTS

5620 ELEMENTS REMAINING

5500 ELEMENTS REMAINING

5000 ELEMENTS REMAINING

4500 ELEMENTS REMAINING

4000 ELEMENTS REMAINING

3500 ELEMENTS REMAINING

3000 ELEMENTS REMAINING

2500 ELEMENTS REMAINING

2000 ELEMENTS REMAINING

1500 ELEMENTS REMAINING

1000 ELEMENTS REMAINING

500 ELEMENTS REMAINING

**** GROUPS REMAINING 1

**** GROUP USED--ELEMENT/GLOBAL CONTRIBUTIONS

4060 ELEMENTS

4060 ELEMENTS REMAINING

4000 ELEMENTS REMAINING

3900 ELEMENTS REMAINING

3800 ELEMENTS REMAINING

3700 ELEMENTS REMAINING

3600 ELEMENTS REMAINING

3500 ELEMENTS REMAINING

3400 ELEMENTS REMAINING

3300 ELEMENTS REMAINING

3200 ELEMENTS REMAINING

3100 ELEMENTS REMAINING

3000 ELEMENTS REMAINING

2900 ELEMENTS REMAINING

2800 ELEMENTS REMAINING

2700 ELEMENTS REMAINING

2600 ELEMENTS REMAINING

2500 ELEMENTS REMAINING

2400 ELEMENTS REMAINING

2300 ELEMENTS REMAINING

2200 ELEMENTS REMAINING

2100 ELEMENTS REMAINING

2000 ELEMENTS REMAINING

1900 ELEMENTS REMAINING

1800 ELEMENTS REMAINING

1700 ELEMENTS REMAINING

1600 ELEMENTS REMAINING

1500 ELEMENTS REMAINING

1400 ELEMENTS REMAINING

1300 ELEMENTS REMAINING

1200 ELEMENTS REMAINING

1100 ELEMENTS REMAINING

1000 ELEMENTS REMAINING

900 ELEMENTS REMAINING

800 ELEMENTS REMAINING

700 ELEMENTS REMAINING

600 ELEMENTS REMAINING

500 ELEMENTS REMAINING

400 ELEMENTS REMAINING

300 ELEMENTS REMAINING

200 ELEMENTS REMAINING

100 ELEMENTS REMAINING

**** ENDING REACTION COMPUTATIONS

Mesh convergence_fine.t7 = 673.555 kilobytes

Mesh convergence_fine.t8 = 1036.812 kilobytes

Mesh convergence_fine.t9 = 0.000 kilobytes

Mesh convergence_fine.t10 = 0.000 kilobytes

Mesh convergence_fine.t11 = 0.188 kilobytes

Mesh convergence_fine.t12 = 673.156 kilobytes

Mesh convergence_fine.t13 = 673.555 kilobytes

Mesh convergence_fine.t14 = 0.000 kilobytes

Mesh convergence_fine.t15 = 0.000 kilobytes

Mesh convergence_fine.t17 = 0.000 kilobytes

Mesh convergence_fine.t51 = 3120.000 kilobytes

Mesh convergence_fine.t52 = 86775.000 kilobytes

Mesh convergence_fine.t54 = 336.602 kilobytes

Mesh convergence_fine.t55 = 11948.293 kilobytes

Mesh convergence_fine.t56 = 23896.586 kilobytes

Mesh convergence_fine.t58 = 673.156 kilobytes

Mesh convergence_fine.t59 = 36854.629 kilobytes

total temporary disk storage (megabytes) = 162.755

Mesh convergence_fine.l = 6.173 kilobytes

Mesh convergence_fine.do = 1382.344 kilobytes

**** BEGIN DELETING TEMPORARY FILES

Processing completed for model:

[E:\Pitt\THESIS\01172006\CUT\Mesh convergence_fine]

**** TEMPORARY FILES DELETED

**** END OF SUCCESSFUL EXECUTION

**** Total actual hard disk space used = 164.111 megabytes

Sub-total elapsed time = 9.726 minutes

ALGOR (R) Stress Calculation Utility

Version 19.00-WIN 20-DEC-2005

**** Memory Dynamically Allocated = 523768 KB

DATE: JANUARY 17, 2006

TIME: 02:30 PM

INPUT.....E:\Pitt\THESIS\01172006\CUT\Mesh convergence_fine

**** BEGIN TYPE-8 DATA INPUT

13000 (85.%) elements

12000 (78.%) elements

11000 (72.%) elements

10000 (65.%) elements

9000 (59.%) elements

8000 (52.%) elements

7000 (46.%) elements

6000 (39.%) elements

5000 (33.%) elements

4000 (26.%) elements

3000 (20.%) elements

2000 (13.%) elements

1000 (7.%) elements

0 (0.%) elements

**** END TYPE-8 DATA INPUT

**** BEGIN TYPE-8 DATA INPUT

3000 (53.%) elements

2000 (35.%) elements

1000 (18.%) elements

0 (0.%) elements

**** END TYPE-8 DATA INPUT

**** BEGIN TYPE-8 DATA INPUT

0 (0.%) elements

**** END TYPE-8 DATA INPUT

**** Writing stress and strain output files ...

**** Hard disk file size information for postprocessor:

Mesh convergence_fine.son = 17160.301 kilobytes

Mesh convergence_fine.nso = 7020.078 kilobytes

Mesh convergence_fine.sto = 7020.078 kilobytes

Total MKNSO disk space used = 30.46920 megabytes

**** End of successful execution

**** MKNSO elapsed time = 0.538 minutes

**** The TOTAL elapsed time = 10.264 minutes

APPENDIX B

SUMMARY FILE FOR CUT CASE 1

ALGOR (R) Static Stress with Linear Material Models

Version 19.00-WIN 20-DEC-2005

DATE: JANUARY 17, 2006

TIME: 02:20 PM

INPUT MODEL: E:\Pitt\THESIS\01172006\CUT\Mesh convergence_fine

PROGRAM VERSION: 19000002

alg.dll VERSION: 19000002

agsdb_ar.dll VERSION: 18000000

algconfig.dll VERSION: 19000000

algsolve.exe VERSION: 19000000

amgsolve.exe VERSION: 03300000

1**** CONTROL INFORMATION

number of node points (NUMNP) = 29489

number of element types (NELTYP) = 3

number of load cases (LL) = 1

number of frequencies (NF) = 0

analysis type code (NDYN) = 0

equations per block (KEQB) = 0

bandwidth minimization flag (MINBND) = 0

gravitational constant (GRAV) = 9.8146E+03

number of equations (NEQ) = 86164

**** PRINT OF NODAL DATA SUPPRESSED

**** PRINT OF EQUATION NUMBERS SUPPRESSED

**** Hard disk file size information for processor:

Available hard disk space on current drive = 7301.895 megabytes

Gravity direction vector = 0.0000E+00 0.0000E+00 -1.0000E+00

1**** ELEMENT LOAD MULTIPLIERS

load case	case A	case B	case C	case D	case E
1	1.000E+00	0.000E+00	0.000E+00	0.000E+00	0.000E+00

**** Invoking Sparse Solver ...

**** Symbolic Assembling Using the Row-Hits Matrix Profile ...

**** Assembled in One Block.

**** Real Sparse Matrix Assembly ...

1**** STIFFNESS MATRIX PARAMETERS

minimum non-zero diagonal element = 1.0229E-02

maximum diagonal element = 7.3595E+01

maximum/minimum = 7.1949E+03

average diagonal element = 8.1394E+00

the minimum is found at equation 18973: node=6489 Tx

the maximum is found at equation 63617: node=21725 Tx

in the upper off-diagonal matrix:

number of entries in the profile = 6708249

number of symbolic nonzero entries= 3145239

number of real nonzero entries = 3144927

**** Sparse Matrix Assembled in One Block

**** Load case 1

**** Sparse Matrix Factorization ...

Completing out-of-core solution (0)

**** Sparse Matrix Solving ...

**** End Sparse Solver Solution

Reaction Sums and Maxima for Load Case 1

Sum of applied forces

X-Force	Y-Force	Z-Force	X-Moment	Y-Moment	Z-Moment
-4.6774E-01	3.9583E-17	1.8771E-04	0.0000E+00	0.0000E+00	0.0000E+00

Sum of reactions

X-Force	Y-Force	Z-Force	X-Moment	Y-Moment	Z-Moment
-1.4303E-14	5.4900E-15	2.0055E-14	0.0000E+00	0.0000E+00	0.0000E+00

Sum of residuals

X-Force	Y-Force	Z-Force	X-Moment	Y-Moment	Z-Moment
-4.6774E-01	5.5254E-15	1.8771E-04	0.0000E+00	0.0000E+00	0.0000E+00

Sum of unfixed direction residuals

X-Force	Y-Force	Z-Force	X-Moment	Y-Moment	Z-Moment
6.8382E-15	-2.2444E-15	2.2467E-14	0.0000E+00	0.0000E+00	0.0000E+00

Largest applied forces and moments

	Node	Node	Node	Node	Node	Node
X-Force	Y-Force	Z-Force	X-Moment	Y-Moment	Z-Moment	
	22502	22511	19179	0	0	0
-6.5178E-04	6.4376E-04	-3.0482E-04	0.0000E+00	0.0000E+00	0.0000E+00	

Largest nodal reactions

	Node	Node	Node	Node	Node	Node
X-Force	Y-Force	Z-Force	X-Moment	Y-Moment	Z-Moment	
	21757	22493	19189	0	0	0
-7.3400E-04	6.4376E-04	3.0482E-04	0.0000E+00	0.0000E+00	0.0000E+00	

Largest nodal residuals

Node	Node	Node	Node	Node	Node
X-Force	Y-Force	Z-Force	X-Moment	Y-Moment	Z-Moment
21757	28372	29489	0	0	0
-7.3400E-04	9.4447E-11	1.8771E-04	0.0000E+00	0.0000E+00	0.0000E+00

Largest unfixed direction residuals

Node	Node	Node	Node	Node	Node
X-Force	Y-Force	Z-Force	X-Moment	Y-Moment	Z-Moment
22230	23270	19456	0	0	0
-1.5613E-15	1.0547E-15	-1.6072E-15	0.0000E+00	0.0000E+00	0.0000E+00

1**** TEMPORARY FILE STORAGE (MEGABYTES)

UNIT NO. 7 :	0.658
UNIT NO. 8 :	1.013
UNIT NO. 9 :	0.000
UNIT NO. 10 :	0.000
UNIT NO. 11 :	0.000
UNIT NO. 12 :	0.657
UNIT NO. 13 :	0.658
UNIT NO. 14 :	0.000
UNIT NO. 15 :	0.000
UNIT NO. 17 :	0.000
UNIT NO. 51 :	3.047
UNIT NO. 52 :	84.741
UNIT NO. 54 :	0.329

UNIT NO. 55 : 11.668

UNIT NO. 56 : 23.337

UNIT NO. 58 : 0.657

UNIT NO. 59 : 35.991

TOTAL : 162.755 Megabytes

APPENDIX C

LOG FILE FOR UNCUT CASE 1

ALGOR (R) Static Stress with Linear Material Models

Version 19.00-WIN 20-DEC-2005

29489 3 1 0 0 0

**** Linear stress analysis

**** Memory Dynamically Allocated = 523768 KB

Options executed are:

NOMIN

STRAIN

SPARSE

SUPCNF

SUPELM

SUPNOD

REAC

ENOR

processing ...

**** OPENING TEMPORARY FILES

NDYN = 0

DATE: JANUARY 17, 2006

TIME: 01:45 PM

INPUT MODEL: E:\Pitt\THESIS\01172006\UNCUT\Mesh convergence_fine

PROGRAM VERSION: 19000002

alg.dll VERSION: 19000002

agsdb_ar.dll VERSION: 18000000

algconfig.dll VERSION: 19000000

algsolve.exe VERSION: 19000000

amgsolve.exe VERSION: 03300000

**** BEGIN NODAL DATA INPUT

29489 NODES

**** END NODAL DATA INPUT

**** BEGIN TYPE-8 data INPUT

PART 1 CONTAINING 15280 ELEMENTS

13000 (85.%) elements

12000 (78.%) elements

11000 (72.%) elements

10000 (65.%) elements

9000 (59.%) elements

8000 (52.%) elements

7000 (46.%) elements

6000 (39.%) elements

5000 (33.%) elements

4000 (26.%) elements

3000 (20.%) elements

2000 (13.%) elements

1000 (7.%) elements

0 (0.%) elements

**** end TYPE-8 data INPUT

**** BEGIN TYPE-8 data INPUT

PART 2 CONTAINING 5620 ELEMENTS

4000 (71.%) elements

3000 (53.%) elements

2000 (35.%) elements

1000 (18.%) elements

0 (0.%) elements

**** end TYPE-8 data INPUT

**** BEGIN TYPE-8 data INPUT

PART 3 CONTAINING 4060 ELEMENTS

2000 (49.%) elements

1000 (25.%) elements

0 (0.%) elements

**** end TYPE-8 data INPUT

**** Hard disk file size information for processor:

Available hard disk space on current drive = 7296.582 megabytes

**** BEGIN LOAD INPUT

Gravity direction vector = 0.0000E+00 0.0000E+00 -1.0000E+00

One load case in 42 blocks.

Load factor = 1.00E+00 in the 1st basket in load case 1

**** END LOAD INPUT

**** Invoking Sparse Solver ...

**** Symbolic Assembling Using the Row-Hits Matrix Profile ...

**** Assembled in One Block.

**** Real Sparse Matrix Assembly ...

in the upper off-diagonal matrix:

number of entries in the profile = 6659296

number of symbolic nonzero entries= 3117143

number of real nonzero entries = 3116831

**** Sparse Matrix Assembled in One Block

**** Load case 1

**** Sparse Matrix Factorization ...

**** Sparse Matrix Solving ...

**** End Sparse Solver Solution

**** BEGIN DISPLACEMENT OUTPUT

**** PRINT OF DISPLACEMENT OUTPUT SUPPRESSED

**** END   DISPLACEMENT OUTPUT

**** BEGINNING REACTION COMPUTATIONS

**** LOADCASES REMAINING   1

**** BLOCKS REMAINING   1

**** GROUPS REMAINING   3

**** GROUP USED--ELEMENT/GLOBAL CONTRIBUTIONS

15280 ELEMENTS

15280 ELEMENTS REMAINING

15000 ELEMENTS REMAINING

14000 ELEMENTS REMAINING

13000 ELEMENTS REMAINING

12000 ELEMENTS REMAINING

11000 ELEMENTS REMAINING

10000 ELEMENTS REMAINING

9000 ELEMENTS REMAINING

8000 ELEMENTS REMAINING

7000 ELEMENTS REMAINING

6000 ELEMENTS REMAINING

5000 ELEMENTS REMAINING

4000 ELEMENTS REMAINING

3000 ELEMENTS REMAINING

2000 ELEMENTS REMAINING

1000 ELEMENTS REMAINING

**** GROUPS REMAINING   2

**** GROUP USED--ELEMENT/GLOBAL CONTRIBUTIONS

5620 ELEMENTS

5620 ELEMENTS REMAINING

5500 ELEMENTS REMAINING

5000 ELEMENTS REMAINING

4500 ELEMENTS REMAINING

4000 ELEMENTS REMAINING

3500 ELEMENTS REMAINING

3000 ELEMENTS REMAINING

2500 ELEMENTS REMAINING

2000 ELEMENTS REMAINING

1500 ELEMENTS REMAINING

1000 ELEMENTS REMAINING

500 ELEMENTS REMAINING

**** GROUPS REMAINING 1

**** GROUP USED--ELEMENT/GLOBAL CONTRIBUTIONS

4060 ELEMENTS

4060 ELEMENTS REMAINING

4000 ELEMENTS REMAINING

3900 ELEMENTS REMAINING

3800 ELEMENTS REMAINING

3700 ELEMENTS REMAINING

3600 ELEMENTS REMAINING

3500 ELEMENTS REMAINING

3400 ELEMENTS REMAINING

3300 ELEMENTS REMAINING

3200 ELEMENTS REMAINING

3100 ELEMENTS REMAINING

3000 ELEMENTS REMAINING

2900 ELEMENTS REMAINING

2800 ELEMENTS REMAINING

2700 ELEMENTS REMAINING

2600 ELEMENTS REMAINING

2500 ELEMENTS REMAINING

2400 ELEMENTS REMAINING

2300 ELEMENTS REMAINING

2200 ELEMENTS REMAINING

2100 ELEMENTS REMAINING

2000 ELEMENTS REMAINING

1900 ELEMENTS REMAINING

1800 ELEMENTS REMAINING

1700 ELEMENTS REMAINING

1600 ELEMENTS REMAINING

1500 ELEMENTS REMAINING

1400 ELEMENTS REMAINING

1300 ELEMENTS REMAINING

1200 ELEMENTS REMAINING

1100 ELEMENTS REMAINING

1000 ELEMENTS REMAINING

900 ELEMENTS REMAINING

800 ELEMENTS REMAINING

700 ELEMENTS REMAINING

600 ELEMENTS REMAINING

500 ELEMENTS REMAINING

400 ELEMENTS REMAINING

300 ELEMENTS REMAINING

200 ELEMENTS REMAINING

100 ELEMENTS REMAINING

**** ENDING REACTION COMPUTATIONS

Mesh convergence_fine.t7 = 669.375 kilobytes

Mesh convergence_fine.t8 = 1036.812 kilobytes

Mesh convergence_fine.t9 = 0.000 kilobytes

Mesh convergence_fine.t10 = 0.000 kilobytes

Mesh convergence_fine.t11 = 0.188 kilobytes

Mesh convergence_fine.t12 = 668.727 kilobytes

Mesh convergence_fine.t13 = 669.375 kilobytes

Mesh convergence_fine.t14 = 0.000 kilobytes

Mesh convergence_fine.t15 = 0.000 kilobytes

Mesh convergence_fine.t17 = 0.000 kilobytes

Mesh convergence_fine.t51 = 3120.000 kilobytes

Mesh convergence_fine.t52 = 86775.000 kilobytes

Mesh convergence_fine.t54 = 334.387 kilobytes

Mesh convergence_fine.t55 = 11840.758 kilobytes

Mesh convergence_fine.t56 = 23681.516 kilobytes

Mesh convergence_fine.t58 = 668.727 kilobytes

Mesh convergence_fine.t59 = 36525.379 kilobytes

total temporary disk storage (megabytes) = 162.100

Mesh convergence_fine.l = 6.176 kilobytes

Mesh convergence_fine.do = 1382.344 kilobytes

**** BEGIN DELETING TEMPORARY FILES

Processing completed for model:

[E:\Pitt\THESIS\01172006\UNCUT\Mesh convergence_fine]

**** TEMPORARY FILES DELETED

**** END OF SUCCESSFUL EXECUTION

**** Total actual hard disk space used = 163.456 megabytes

Sub-total elapsed time = 6.502 minutes

ALGOR (R) Stress Calculation Utility

Version 19.00-WIN 20-DEC-2005

**** Memory Dynamically Allocated = 523768 KB

DATE: JANUARY 17, 2006

TIME: 01:51 PM

INPUT.....E:\Pitt\THESIS\01172006\UNCUT\Mesh convergence_fine

**** BEGIN TYPE-8 DATA INPUT

12000 (78.%) elements

10000 (65.%) elements

8000 (52.%) elements

6000 (39.%) elements

4000 (26.%) elements

2000 (13.%) elements

0 (0.%) elements

**** END TYPE-8 DATA INPUT

**** BEGIN TYPE-8 DATA INPUT

2000 (35.%) elements

0 (0.%) elements

**** END TYPE-8 DATA INPUT

**** BEGIN TYPE-8 DATA INPUT

2000 (49.%) elements

0 (0.%) elements

**** END TYPE-8 DATA INPUT

**** Writing stress and strain output files ...

**** Hard disk file size information for postprocessor:

Mesh convergence_fine.son = 17160.301 kilobytes

Mesh convergence_fine.nso = 7020.078 kilobytes

Mesh convergence_fine.sto = 7020.078 kilobytes

Total MKNSO disk space used = 30.46920 megabytes

**** End of successful execution

**** MKNSO elapsed time = 0.477 minutes

**** The TOTAL elapsed time = 6.979 minutes

APPENDIX D

SUMMARY FILE FOR UNCUT CASE 1

ALGOR (R) Static Stress with Linear Material Models

Version 19.00-WIN 20-DEC-2005

DATE: JANUARY 17, 2006

TIME: 01:45 PM

INPUT MODEL: E:\Pitt\THESIS\01172006\UNCUT\Mesh convergence_fine

PROGRAM VERSION: 19000002

alg.dll VERSION: 19000002

agsdb_ar.dll VERSION: 18000000

algconfig.dll VERSION: 19000000

algsolve.exe VERSION: 19000000

amgsolve.exe VERSION: 03300000

1**** CONTROL INFORMATION

number of node points (NUMNP) = 29489

number of element types (NELTYP) = 3

number of load cases (LL) = 1

number of frequencies (NF) = 0

analysis type code (NDYN) = 0

equations per block (KEQB) = 0

bandwidth minimization flag (MINBND) = 0

gravitational constant (GRAV) = 9.8146E+03

number of equations (NEQ) = 85597

**** PRINT OF NODAL DATA SUPPRESSED

**** PRINT OF EQUATION NUMBERS SUPPRESSED

**** Hard disk file size information for processor:

Available hard disk space on current drive = 7296.582 megabytes

Gravity direction vector = 0.0000E+00 0.0000E+00 -1.0000E+00

1**** ELEMENT LOAD MULTIPLIERS

load case	case A	case B	case C	case D	case E
1	1.000E+00	0.000E+00	0.000E+00	0.000E+00	0.000E+00

**** Invoking Sparse Solver ...

**** Symbolic Assembling Using the Row-Hits Matrix Profile ...

**** Assembled in One Block.

**** Real Sparse Matrix Assembly ...

1**** STIFFNESS MATRIX PARAMETERS

minimum non-zero diagonal element = 1.2121E-02

maximum diagonal element = 7.3595E+01

maximum/minimum = 6.0718E+03

average diagonal element = 8.1926E+00

the minimum is found at equation 43704: node=15062 Tz

the maximum is found at equation 63050: node=21725 Tx

in the upper off-diagonal matrix:

number of entries in the profile = 6659296

number of symbolic nonzero entries= 3117143

number of real nonzero entries = 3116831

**** Sparse Matrix Assembled in One Block

**** Load case 1

**** Sparse Matrix Factorization ...

Completing out-of-core solution (0)

**** Sparse Matrix Solving ...

**** End Sparse Solver Solution

Reaction Sums and Maxima for Load Case 1

Sum of applied forces

X-Force	Y-Force	Z-Force	X-Moment	Y-Moment	Z-Moment
-4.6774E-01	3.9583E-17	1.8771E-04	0.0000E+00	0.0000E+00	0.0000E+00

Sum of reactions

X-Force	Y-Force	Z-Force	X-Moment	Y-Moment	Z-Moment
-2.3484E-15	6.5661E-15	-1.1137E-14	0.0000E+00	0.0000E+00	0.0000E+00

Sum of residuals

X-Force	Y-Force	Z-Force	X-Moment	Y-Moment	Z-Moment
-4.6774E-01	6.6067E-15	1.8771E-04	0.0000E+00	0.0000E+00	0.0000E+00

Sum of unfixed direction residuals

X-Force	Y-Force	Z-Force	X-Moment	Y-Moment	Z-Moment
2.3668E-14	9.5850E-15	-1.2355E-14	0.0000E+00	0.0000E+00	0.0000E+00

Largest applied forces and moments

	Node	Node	Node	Node	Node	Node
X-Force	22502	22511	19179	0	0	0
Y-Force	-6.5178E-04	6.4376E-04	-3.0482E-04	0.0000E+00	0.0000E+00	0.0000E+00
Z-Force						
X-Moment						
Y-Moment						
Z-Moment						

Largest nodal reactions

	Node	Node	Node	Node	Node	Node
X-Force	21777	22493	19179	0	0	0
Y-Force	-7.3399E-04	6.4376E-04	3.0482E-04	0.0000E+00	0.0000E+00	0.0000E+00
Z-Force						
X-Moment						
Y-Moment						
Z-Moment						

Largest nodal residuals

Node	Node	Node	Node	Node	Node
X-Force	Y-Force	Z-Force	X-Moment	Y-Moment	Z-Moment
21777	29489	29489	0	0	0
-7.3399E-04	-9.4339E-11	1.8771E-04	0.0000E+00	0.0000E+00	0.0000E+00

Largest unfixed direction residuals

Node	Node	Node	Node	Node	Node
X-Force	Y-Force	Z-Force	X-Moment	Y-Moment	Z-Moment
23405	21418	21206	0	0	0
-1.6168E-15	1.0200E-15	1.5266E-15	0.0000E+00	0.0000E+00	0.0000E+00

1**** TEMPORARY FILE STORAGE (MEGABYTES)

UNIT NO. 7 : 0.654

UNIT NO. 8 : 1.013

UNIT NO. 9 : 0.000

UNIT NO. 10 : 0.000

UNIT NO. 11 : 0.000

UNIT NO. 12 : 0.653

UNIT NO. 13 : 0.654

UNIT NO. 14 : 0.000

UNIT NO. 15 : 0.000

UNIT NO. 17 : 0.000

UNIT NO. 51 : 3.047

UNIT NO. 52 : 84.741

UNIT NO. 54 : 0.327

UNIT NO. 55 : 11.563

UNIT NO. 56 : 23.126

UNIT NO. 58 : 0.653

UNIT NO. 59 : 35.669

TOTAL : 162.100 Megabytes

APPENDIX E

SCRIPT FILE FOR NODAL RESULTS

```
Option Explicit

    ' alg_rb.ResultsBrowser constants
    Const OCDisplacement = 0 ' Output Calculation Type
    Const UOpNone        = 0 ' Unary Operator

    ' Get the displacement vector at node x in load case 1
    Call    GetNodeVectorResults("E:\Pitt\THESIS\04032006\CASE    1\CUT\Plate-Nerve.esx",    OCDisplacement,
            UOpNone, 1, 12)
    Call    GetNodeVectorResults("E:\Pitt\THESIS\04032006\CASE    1\CUT\Plate-Nerve.esx",    OCDisplacement,
            UOpNone, 1, 22)
    Call    GetNodeVectorResults("E:\Pitt\THESIS\04032006\CASE    1\CUT\Plate-Nerve.esx",    OCDisplacement,
            UOpNone, 1, 666)
    Call    GetNodeVectorResults("E:\Pitt\THESIS\04032006\CASE    1\CUT\Plate-Nerve.esx",    OCDisplacement,
            UOpNone, 1, 847)
    Call    GetNodeVectorResults("E:\Pitt\THESIS\04032006\CASE    1\CUT\Plate-Nerve.esx",    OCDisplacement,
            UOpNone, 1, 646)
    Call    GetNodeVectorResults("E:\Pitt\THESIS\04032006\CASE    1\CUT\Plate-Nerve.esx",    OCDisplacement,
            UOpNone, 1, 3717)
```

```
Call GetNodeVectorResults("E:\Pitt\THESIS\04032006\CASE 1\UNCUT\Plate-Nerveu1.esx", OCDisplacement,
        UOpNone, 1, 12)
Call GetNodeVectorResults("E:\Pitt\THESIS\04032006\CASE 1\UNCUT\Plate-Nerveu1.esx", OCDisplacement,
        UOpNone, 1, 22)
Call GetNodeVectorResults("E:\Pitt\THESIS\04032006\CASE 1\UNCUT\Plate-Nerveu1.esx", OCDisplacement,
        UOpNone, 1, 666)
Call GetNodeVectorResults("E:\Pitt\THESIS\04032006\CASE 1\UNCUT\Plate-Nerveu1.esx", OCDisplacement,
        UOpNone, 1, 847)
Call GetNodeVectorResults("E:\Pitt\THESIS\04032006\CASE 1\UNCUT\Plate-Nerveu1.esx", OCDisplacement,
        UOpNone, 1, 646)
Call GetNodeVectorResults("E:\Pitt\THESIS\04032006\CASE 1\UNCUT\Plate-Nerveu1.esx", OCDisplacement,
        UOpNone, 1, 3717)

Sub GetNodeVectorResults(strFeaModelName, OutputCalculation, UnaryOperator, lLoadCase, lNodeNumber)

   ' Local variables
   Dim rb         ' As alg_rbLib.ResultsBrowser
   Dim colNodes   ' As alg_rbLib.Nodes
   Dim objNode    ' As alg_rbLib.Node
   Dim colVectors ' As alg_rbLib.Vectors
   Dim objVector  ' As alg_rbLib.Vector
   Dim strResult  ' As String
   Dim strX       ' As String
   Dim strY       ' As String
   Dim strZ       ' As String
```

```
strResult = "An error occured."

' Create a new ResultsBrowser object
Set rb = CreateObject("alg_rb.ResultsBrowser")
If Not rb Is Nothing Then

   ' Opening the model
   rb.Open strFeaModelName

   ' Set the load case
   rb.LoadCaseNumber = lLoadCase

   ' Create a collection of nodes to hold the result locations
   Set colNodes = CreateObject("alg_rb.Nodes")
   If Not colNodes Is Nothing Then

      ' Create an object to hold the node of interest
      Set objNode = CreateObject("alg_rb.Node")
      If Not objNode Is Nothing Then

         ' Fill in the Node object
         objNode.NodeNumber = lNodeNumber

         ' Add the object to the location collection
         colNodes.Add objNode

         ' Retrieve the results for each of the locations in the collection
         Set colVectors = rb.GetNodeVectorResults(OutputCalculation, _
```

```
                                UnaryOperator, _
                                colNodes)
If Not colVectors Is Nothing Then

   If colVectors.Count Then

      Set objVector = colVectors.Item(0)
      If Not objVector Is Nothing Then

         strX = strY = strZ = "Nan"
         If Not objVector.IsXNAN Then strX = objVector.X
         If Not objVector.IsYNAN Then strY = objVector.Y
         If Not objVector.IsZNAN Then strZ = objVector.Z

         strResult = "The displacement vector at node " & lNodeNumber & _
                  " is " & strX & ", " & strY  & ", " & strZ & "."

         Set objVector = Nothing

      End If

   End If

   Set colVectors = Nothing

End If

Set objNode = Nothing
```

```
        End If

        Set colNodes = Nothing

    End If

    rb.Close

    Set rb = Nothing

End If


    Dim fso, f, ForAppending

    ForAppending = 8

    Set fso = CreateObject("Scripting.FileSystemObject")

    'Set f = fso.CreateTextFile("e:\CASE 1.txt", ForAppending, True)
    Set f = fso.OpenTextFile ("e:\CASE 1.txt", ForAppending, True)

    f.Writeline strResult
    f.Close


'MsgBox strResult
```

```
End Sub
```

BIBLIOGRAPHY

1. Baseline and early natural history report. The Central Vein Occlusion Study.*Arch Ophthalmol* 1993;111:1087-95.

2. Elman MJ. Thrombolytic therapy for central retinal vein occlusion: results of a pilot study. *Trans Am Ophthalmol Soc* 1996;94:471-504.

3. Singh Hayreh S, Opremcak EM, Bruce RA et al. Radial optic neurotomy for central retinal vein obstruction. *Retina* 2002;22:374-7; author reply 377-9.

4. Martinez-Jardon CS, Meza-de Regil A, Dalma-Weiszhausz J et al. Radial optic neurotomy for ischaemic central vein occlusion. *Br J Ophthalmol* 2005;89:558-61.

5. Green WR, Chan CC, Hutchins GM, Terry JM. Central retinal vein occlusion: a prospective histopathologic study of 29 eyes in 28 cases. 1981. *Retina* 2005;25:27-55.

6. Pe'er J, Folberg R, Itin A, Gnessin H, Hemo I, Keshet E. Vascular endothelial growth factor upregulation in human central retinal vein occlusion. *Ophthalmology* 1998;105:412-6.

7. Chen CH, Lai CH, Kuo HK. Laser chorioretinal venous anastomosis for progressive nonischemic central retinal vein occlusion. *Chang Gung Med J* 2005;28:866-71.

8. Guven D, Sayinalp N, Kalayci D, Dundar S, Hasiripi H. Risk factors in central retinal vein occlusion and activated protein C resistance. *Eur J Ophthalmol* 1999;9:43-8.

9. Ip MS, Gottlieb JL, Kahana A et al. Intravitreal triamcinolone for the treatment of macular edema associated with central retinal vein occlusion. *Arch Ophthalmol* 2004;122:1131-6.

10. Hattenbach LO, Steinkamp G, Scharrer I, Ohrloff C. Fibrinolytic therapy with low-dose recombinant tissue plasminogen activator in retinal vein occlusion. *Ophthalmologica* 1998;212:394-8.

11. Hayreh SS. Radial optic neurotomy for nonischemic central retinal vein occlusion. *Arch Ophthalmol* 2004;122:1572-3.

12. Opremcak EM, Bruce RA, Lomeo MD, Ridenour CD, Letson AD, Rehmar AJ. Radial optic neurotomy for central retinal vein occlusion: a retrospective pilot study of 11 consecutive cases. *Retina* 2001;21:408-15.

13. Soheilian M, Koochek A, Yazdani S, Peyman GA. Transvitreal optic neurotomy for nonarteritic anterior ischemic optic neuropathy. *Retina* 2003;23:692-7.

14. Garciia-Arumii J, Boixadera A, Martinez-Castillo V, Castillo R, Dou A, Corcostegui B. Chorioretinal anastomosis after radial optic neurotomy for central retinal vein occlusion. *Arch Ophthalmol* 2003;121:1385-91.

15. Nomoto H, Shiraga F, Yamaji H et al. Evaluation of radial optic neurotomy for central retinal vein occlusion by indocyanine green videoangiography and image analysis. *Am J Ophthalmol* 2004;138:612-9.

16. Vonesh MJ, Cho CH, Pinto JV, Jr. et al. Regional vascular mechanical properties by 3-D intravascular ultrasound with finite-element analysis. *Am J Physiol* 1997;272:H425-37.

17. Mower WR, Baraff LJ, Sneyd J. Stress distributions in vascular aneurysms: factors affecting risk of aneurysm rupture. *J Surg Res* 1993;55:155-61.

18. Stringfellow MM, Lawrence PF, Stringfellow RG. The influence of aorta-aneurysm geometry upon stress in the aneurysm wall. *J Surg Res* 1987;42:425-33.

19. Edwards ME, Good TA. Use of a mathematical model to estimate stress and strain during elevated pressure induced lamina cribrosa deformation. *Curr Eye Res* 2001;23:215-25.

20. Schneider U, Inhoffen W, Grisanti S, Volker M, Bartz-Schmidt KU. Chorioretinal neovascularization after radial optic neurotomy for central retinal vein occlusion. *Ophthalmic Surg Lasers Imaging* 2005;36:508-11.

21. Belli S, Eskitascioglu G, Eraslan O, Senawongse P, Tagami J. Effect of hybrid layer on stress distribution in a premolar tooth restored with composite or ceramic inlay: an FEM study. *J Biomed Mater Res B Appl Biomater* 2005;74:665-8.

22. Friberg TR, Lace JW. A comparison of the elastic properties of human choroid and sclera. *Exp Eye Res* 1988;47:429-36.

23. Friberg TR. The etiology of choroidal folds. A biomechanical explanation. *Graefes Arch Clin Exp Ophthalmol* 1989;227:459-64.

24. Hayreh SS. Radial optic neurotomy for central retinal vein occlusion. *Retina* 2002;22:827; author reply 827.

25. Tao Y, Jiang YR, Li XX, Yin CY, Yao J. Fundus and histopathological study of radial optic neurotomy in the normal miniature pig eye. *Arch Ophthalmol* 2005;123:1097-101.

26. Wrede J, Varadi G, Volcker HE, Dithmar S. [Radial optic neurotomy for central retinal vein occlusion - how deep should it be?]. *Ophthalmologe* 2005.

27. Yamamoto S, Takatsuna Y, Sato E, Mizunoya S. Central retinal artery occlusion after radial optic neurotomy in a patient with central retinal vein occlusion. *Am J Ophthalmol* 2005;139:206-7.

28. Samuel MA, Desai UR, Gandolfo CB. Peripapillary retinal detachment after radial optic neurotomy for central retinal vein occlusion. *Retina* 2003;23:580-3.

29. Horio N, Horiguchi M. Central retinal vein occlusion with further reduction of retinal blood flow one year after radial optic neurotomy. *Am J Ophthalmol* 2005;139:926-7.